Journal of Computational Physics 507 (2024) 112975

Contents lists available at ScienceDirect

Journal of Computational Physics

journal homepage: www.elsevier.com/locate/jcp

DOT-type schemes for hybrid hyperbolic problems arising from free-surface, mobile-bed, shallow-flow models

Daniel Zugliani *, Giorgio Rosatti

Department of Civil, Environmental and Mechanical Engineering - University of Trento, via Mesiano, 77, Trento, 38123, TN, Italy

ARTICLE INFO

Keywords:
Osher-type flux
DOT-type flux
Hybrid system
Free-surface shallow flow
Debris-flow model
Non-conservative term

ABSTRACT

Free-surface, mobile-bed, shallow-flow models may present Hybrid hyperbolic systems of partial differential equations characterised by conservative and non-conservative fluxes that can only be expressed in primitive variables. This paper presents the effort we made to derive DOT-type schemes (Osher-type schemes derived by Dumbser and Toro, 2011 [1]) for these kinds of systems formulated for the one-dimensional case. Firstly, for a Hybrid system, we managed to write a quasi-linear form characterised by the presence of a matrix, expressed as a function of the primitive variables, that multiplies the spatial derivative of the conserved variables. Next, we derived the first numerical flux by adapting the approach of Leibinger et al., 2016 [2] to this quasi-linear form. We called this result DOT_{HCP} flux. To achieve a faster algorithm, instead of using an integration path in the space of conserved variables, as in the previous case, we employed a path in the space of primitive variables. We called this second formulation DOT_{HPP} flux. Subsequently, we managed to account for certain physical constraints arising from the generalised Rankine-Hugoniot relations in the expression of one term of the previous flux formulation, thus obtaining the DOT_{HZR} flux. Finally, we showed that these methods can also be applied to Combined systems characterised by conservative and non-conservative fluxes expressed in conserved variables. Several tests show the characteristics and good performances of the proposed methods when applied to Riemann problems of Hybrid and Combined systems deriving from free-surface models. Finally, thanks to the general formulation of the proposed DOT-type fluxes, these can also be applied to Hybrid and Combined hyperbolic systems deriving from different physical problems.

1. Introduction

Free-surface, shallow flows constitute a broad class of gravity-driven geophysical fluid motions characterized by a vertical scale much smaller than the horizontal size of the flow domain. Although water flows are the most studied situations, many other phenomena are of interest in environmental fluid dynamics. A convenient classification of them can be based on the number of phases (namely, the constituents) used to describe the flow with a given degree of approximation:

- mono-phase models: despite the actual number of constituents, the flow is described by employing only one phase. Among many, there are the avalanche models of Christen et al. [3] and Zugliani and Rosatti [4], the overland flow models of Costabile et al. [5], Singh et al. [6] and Fernández-Pato et al. [7] or the mud-flow model of O'Brien et al. [8];

* Corresponding author.
E-mail addresses: daniel.zugliani@unitn.it (D. Zugliani), giorgio.rosatti@unitn.it (G. Rosatti).

https://doi.org/10.1016/j.jcp.2024.112975
Received 25 October 2023; Received in revised form 24 February 2024; Accepted 25 March 2024

Available online 28 March 2024

Table 1
Classes of PDE system with the relevant equation written in compact form.

System class	Equation
Conservative	$\frac{\partial \mathbf{U}}{\partial t} + \frac{\partial \mathbf{F}}{\partial x} = \mathbf{S}$
Non-conservative	$\frac{\partial \mathbf{U}}{\partial t} + \mathbf{H}_U \frac{\partial \mathbf{U}}{\partial x} = \mathbf{S}$
Combined	$\frac{\partial \mathbf{U}}{\partial t} + \frac{\partial \mathbf{F}}{\partial x} + \mathbf{H}_U \frac{\partial \mathbf{U}}{\partial x} = \mathbf{S}$
Hybrid	$\frac{\partial \mathbf{U}}{\partial t} + \frac{\partial \mathbf{F}}{\partial x} + \mathbf{H}_W \frac{\partial \mathbf{W}}{\partial x} = \mathbf{S}$

- two-phase models: two distinct constituents interacting with each other describe the flow in this case. Some examples are the hyper-concentrated and debris flow models of Armanini et al. [9] and Bouchut et al. [10] or the mobile bed models of Rosatti and Zugliani [11] and Di Cristo et al. [12];
- three-phase models: examples of this class are the rock-ice model of Sansone et al. [13], the fluid-air-sediment models of Ouda and Toorman [14] or the liquid with fine and coarse solids model of Pudasaini and Mergili [15].

Other flows, composed of four or more components, could be classified as multi-phase models and sometimes are extensions of the two- or three-phase models.

Typically, a shallow flow is described using a depth-averaged approach. The relevant mathematical model is characterised by a hyperbolic system of N Partial Differential Equations (PDEs) plus some algebraic relations, where PDEs derive primarily from mass (or volume) and momentum balances for each phase (or combination of them) [13]. For simplicity, here we consider only the pure one-dimensional case, whose relative generic system, in compact form, may be written in the following way:

$$\frac{\partial \mathbf{U}}{\partial t} + \frac{\partial \mathbf{F}}{\partial x} + \mathbf{H}_U \frac{\partial \mathbf{U}}{\partial x} + \mathbf{H}_W \frac{\partial \mathbf{W}}{\partial x} = \mathbf{S} \tag{1}$$

where $\mathbf{U}$ is the vector of conserved variables (here, the adjective *conserved* is related more to the physical than the mathematical meaning since we are in a context of non-conservative sets), $\mathbf{W}$ is the vector of primitive variables, $\mathbf{F}$ is the vector of conservative fluxes, $\mathbf{H}_U \partial \mathbf{U}/\partial x$ and $\mathbf{H}_W \partial \mathbf{W}/\partial x$ are non-conservative products where $\mathbf{H}_U$ and $\mathbf{H}_W$ are matrices expressed as a function of the conserved and primitive variables respectively, and finally $\mathbf{S}$ is the vector of source terms. The non-conservative products are commonly called non-conservative fluxes and are not well-defined even as distributions in case of discontinuity. To make mathematical sense of them, it is necessary to resort to the theory proposed by Dal Maso et al. [16] and widely used in the literature [e.g., 17–19]. We distinguish here two types of non-conservative fluxes because in some models, as shown further on, we can write both the non-conservative terms and the conservative fluxes only as a function of the primitive variables since it is impossible to explicitly express the primitive variables as a function of the conserved one, the relevant relation being a non-linear system without an explicit solution. We call this kind of PDE system *Hybrid system*. On the contrary, systems in which both conservative and non-conservative terms can be written as a function of the conserved variables are defined by Leibinger et al. [2] as *Combined systems*. Since not all the terms in Eq. (1) are simultaneously present in each of the models cited, we can distinguish four different classes of systems depending on the terms actually present on its left-hand side, as reported in Table 1.

From a numerical point of view, considering a spatial domain divided into cells of constant width Δx, being $i\Delta x$ the centre of the i-th cell, a generic first order finite volume discretization of the system (1) can be written as follows:

$$\mathbf{U}_i^{n+1} = \mathbf{U}_i^n - \frac{\Delta t}{\Delta x}\left(\mathbf{F}_{i+1/2}^- - \mathbf{F}_{i-1/2}^+\right) + \Delta t \mathbf{S}_i \tag{2}$$

where $\mathbf{U}_i^{n+1}$ is the averaged value of the conserved variable vector inside the i-th cell at time $t = (n+1)\Delta t$, $\mathbf{U}_i^n$ is the value of the same vector at time $t = n\Delta t$, Δt is the time step, and $\mathbf{S}_i$ is the averaged value of the source terms inside the cell. Finally, in the framework of Godunov method, $\mathbf{F}_{i\pm1/2}^{\mp}$ are the side fluxes evaluated from suitable approximate solutions of the Riemann Problems (RPs) generated on the cell interfaces. It should be noted that these terms may include both conservative and non-conservative fluxes. Some examples of this type of numerical approach are present in Fraccarollo et al. [20], Murillo and García-Navarro [21,22], Castro Díaz et al. [23], Rosatti and Begnudelli [24], Castro et al. [25], among many others.

Due to the peculiar characteristic of the PDE system describing some free-surface shallow flow, with particular attention to the debris flow model (see Section 2.2), this work aims to derive DOT-type schemes tailored and optimized explicitly for Hybrid systems, also applicable to Combined systems. The DOT-type schemes derive from the works of Dumbser and Toro [26,1] in which Osher's original approach [27] was improved and extended to the cases of Conservative or Non-conservative systems, respectively. We achieved our result firstly, by being able to write a quasi-linear form characterised by the presence of a matrix, expressed as a function of the primitive variables, that multiplies the spatial derivative of the conserved variables, then exploiting the possibility of expressing the integrals present in DOT-type schemes, originally defined in the conserved variable phase space by Dumbser and Toro [26,1], in integrals defined in the primitive variable phase space. Furthermore, we succeeded in accounting for some physical constraints arising from the Generalised Rankine-Hugoniot (GRH) relations in the expression of one term of the novel flux formulation.

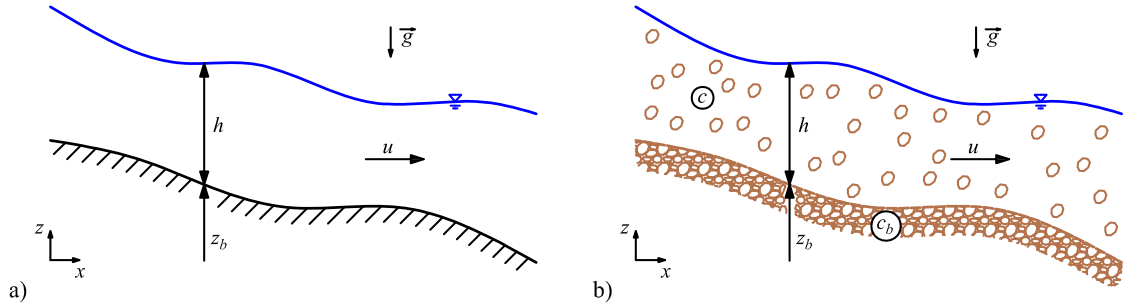

Fig. 1. Sketch of the main variables involved in the free surface models considered in this paper: a) overland flow, b) debris flow.

The proposed schemes were developed within a first-order finite volume framework, as we wanted to focus mainly on the basic approach and highlight its potential. For the same reason, we only considered the homogeneous part of Eq. (1), as we can easily account for the source term using the operator splitting technique [28,4]. Obviously, these schemes can be a starting point for higher-order methods, but we will address this in future work.

To show the performance of the new DOT-type schemes, we applied them to the Hybrid system describing a two-phase debris flow over a mobile bed and to the Combined system describing a mono-phase overland flow over a fixed bed. We choose these two types of flow problems because, in their two-dimensional formulations, they are helpful in many practical situations, such as designing hydraulic defence structures (e.g., levee and check dams), defining hazard mapping and passive mitigation strategies for hydro-geological events (e.g., emergency plans) or perform back-analysis of complex debris flow events (e.g., the clogging of a culvert [29]).

The paper is structured as follows: Section 2 briefly describes the overland and the debris flow models along with some specific features exploited in the novel schemes; Section 3 presents a summary of the original Osher approach and some of its extensions present in the literature; Section 4 deals with our novel DOT-type schemes for Hybrid hyperbolic systems while Sections 5 and 6 illustrate the application of the developed schemes to debris flow and overland flow Test cases, respectively. Conclusions end the paper.

2. The PDEs systems and the GRH relations for the overland and debris flow models

In this Section, we describe the PDE systems of the overland and debris flow models, their compact expression in the form of Eq. (1) and the relevant GRH relations that will be used in the novel schemes.

2.1. The 1D overland flow model

The 1D overland flow model describes the motion of a mono-phase fluid (usually water), with constant density ρ, over a fixed topography. Referring to Fig. 1a), the relevant PDE system is:

$$\begin{cases} \dfrac{\partial}{\partial t}\left(h+z_b\right)+\dfrac{\partial}{\partial x}\left(uh\right)=0 \\ \dfrac{\partial}{\partial t}\left(uh\right)+\dfrac{\partial}{\partial x}\left(u^2h+g\dfrac{h^2}{2}\right)+gh\dfrac{\partial}{\partial x}(z_b)=-\dfrac{\tau_0}{\rho} \\ \dfrac{\partial}{\partial t}(z_b)=0 \end{cases} \tag{3}$$

where x is the horizontal direction, t is the time, h is the flow depth, z_b is the bed elevation, u is the depth-averaged velocity, g is the module of gravity acceleration assumed constant and equal to $g=9.81\,\mathrm{m/s^2}$, and τ_0 is the bed shear stress. The first two equations in system (3) express the mass and the momentum balance of the flowing fluid, while the last one expresses the time invariance of bed elevation. The last equation is useful when dealing with discontinuous bed elevation, as demonstrated in [30,31,19].

Considering the vector of primitive variables $\mathbf{W}^T=[h,u,z_b]^T$, it is possible to express the conserved variables vector as a function of the primitive one:

$$\mathbf{U}=\begin{bmatrix}U_1\\U_2\\U_3\end{bmatrix}=\begin{bmatrix}h+z_b\\uh\\z_b\end{bmatrix} \tag{4}$$

Analogously, we can reverse the relation and write the primitive variables vector as a function of the conserved one:

$$\mathbf{W} = \begin{bmatrix} U_1 - U_3 \\ \dfrac{U_2}{U_1 - U_3} \\ U_3 \end{bmatrix} \tag{5}$$

We can now write system (3) in compact form as in (1) using only the conserved variables. The relevant quantities become:

$$\mathbf{F} = \begin{bmatrix} U_2 \\ \dfrac{U_2^2}{U_1 - U_3} + g\dfrac{(U_1 - U_3)^2}{2} \\ 0 \end{bmatrix}; \ \mathbf{H}_U = \begin{bmatrix} 0 & 0 & 0 \\ 0 & 0 & g(U_1 - U_3) \\ 0 & 0 & 0 \end{bmatrix}; \ \mathbf{H}_W = \begin{bmatrix} 0 & 0 & 0 \\ 0 & 0 & 0 \\ 0 & 0 & 0 \end{bmatrix}; \ \mathbf{S} = \begin{bmatrix} 0 \\ -\dfrac{\tau_0}{\rho} \\ 0 \end{bmatrix} \tag{6}$$

Therefore, since the matrix relevant to the non-conservative fluxes expressed as a function of the primitive variables is null, according to the classification presented in Table 1, this system belongs to the class of Combined systems.

The homogeneous part of the system (3) has a complete set of eigenvalues and eigenvectors (see Appendix A for their expressions), and the relevant GRH relation [31,11] for a generic discontinuity is:

$$\mathbf{F}_R - \mathbf{F}_L - \mathbf{D}(\mathbf{W}_L, \mathbf{W}_R) = S_S(\mathbf{U}_R - \mathbf{U}_L) \tag{7}$$

where S_S is the speed of the discontinuity, and the vectors with subscripts R and L refer to their values on the right and left of the discontinuity, respectively. Moreover, $\mathbf{D} = [0, D, 0]^T$ where D is the thrust exerted by the fluid on the bed step [31]. A possible simple expression for D, based on the physics of the problem, is the one proposed in [32] that reads:

$$\begin{aligned} D &= -g\left(h_k - \frac{|z_{b,R} - z_{b,L}|}{2}\right)(z_{b,R} - z_{b,L}) \\ k &= \begin{cases} L & \text{if } z_{b,L} \le z_{b,R} \\ R & \text{otherwise} \end{cases} \end{aligned} \tag{8}$$

We highlight that this expression is valid for many cases, but for specific situations, it can generate non-physical solutions [31,33]. On the other hand, a general physically-based, reliable expression is still missing in the literature. Therefore, a general numerical scheme must not rely on specific properties of the D term to be ready for future, more appropriate expressions.

2.2. The 1D, mobile-bed, debris flow model

The debris flow model used in this work is the pure 1D version of the model of Armanini et al. [9], and it describes the motion of a mixture of water and sediment over a mobile bed under the assumption that the velocity of the two phases is equal (i.e. isokinetic assumption). Referring to Fig. 1b), the relevant PDE system is:

$$\begin{cases} \dfrac{\partial}{\partial t}(h + z_b) + \dfrac{\partial}{\partial x}(uh) = 0 \\ \dfrac{\partial}{\partial t}(1 + c\Delta)uh + \dfrac{\partial}{\partial x}(1 + c\Delta)\left(u^2 h + g\dfrac{h^2}{2}\right) + gh(1 + c\Delta)\dfrac{\partial}{\partial x} z_b = -\dfrac{\tau_0}{\rho} \\ \dfrac{\partial}{\partial t}(ch + c_b z_b) + \dfrac{\partial}{\partial x}(cuh) = 0 \end{cases} \tag{9}$$

where x, t, h, z_b, u, g, and τ_0 have the same meaning as in the previous model while Δ is the constant, relative submerged density of the solid phase defined as $\Delta = (\rho_s - \rho)/\rho$, ρ and ρ_s are the liquid and the solid density, respectively, and c_b is the constant concentration of the solid material in the bed. Finally, c is the depth-averaged concentration of the solid phase in the flow and is expressed by an algebraic relation linking the concentration with the hydrodynamic variables as follows:

$$c = \beta\frac{u^2}{gh} \tag{10}$$

where β is a constant, dimensionless transport parameter.

Considering this last equation and the vector of primitive variables $\mathbf{W}^T = [h, u, z_b]^T$, we can express the conserved variables as a function of the primitive ones:

$$\mathbf{U} = \begin{bmatrix} U_1 \\ U_2 \\ U_3 \end{bmatrix} = \begin{bmatrix} h + z_b \\ \left(1 + \beta\Delta\dfrac{u^2}{gh}\right)uh \\ \beta\dfrac{u^2}{g} + c_b z_b \end{bmatrix} \tag{11}$$

Compared to the overland flow model, the inverse relation can not be evaluated analytically. Therefore, to rewrite the system (9) in compact form, we are forced to keep it in terms of primitive variables:

$$\mathbf{F}=\begin{bmatrix} uh \\ \left(1+\beta\Delta\frac{u^2}{gh}\right)\left(u^2h+g\frac{h^2}{2}\right) \\ cuh \end{bmatrix};\ \mathbf{H}_U=\begin{bmatrix} 0 & 0 & 0 \\ 0 & 0 & 0 \\ 0 & 0 & 0 \end{bmatrix};\ \mathbf{H}_W=\begin{bmatrix} 0 & 0 & 0 \\ 0 & 0 & \left(1+\beta\Delta\frac{u^2}{gh}\right)gh \\ 0 & 0 & 0 \end{bmatrix};\ \mathbf{S}=\begin{bmatrix} 0 \\ -\frac{\tau_0}{\rho} \\ 0 \end{bmatrix} \tag{12}$$

Since matrix $\mathbf{H}_U$ is null, according to the classification presented in Table 1, this system belongs to the class of Hybrid systems.

The homogeneous part of system (9) has a complete set of eigenvalues and eigenvectors (see Appendix B for their expressions) and the GRH relation for a discontinuity is expressed again by Eq. (7), where a physically-based expression for term D is the one proposed in [32]:

$$\begin{aligned} D &= -g\left(1+c_k\Delta\right)\left(h_k-\frac{\left|z_{b,R}-z_{b,L}\right|}{2}\right)\left(z_{b,R}-z_{b,L}\right) \\ k &= \begin{cases} L & \text{if } z_{b,L}\le z_{b,R} \\ R & \text{otherwise} \end{cases} \end{aligned} \tag{13}$$

3. The Osher-type schemes

The Osher-Solomon numerical scheme for conservative systems, leading to the so-called Osher flux, was developed by Osher and Solomon [27] as an extension to the non-linear scalar case of the method of Engquist and Osher [34]. In this Section, we present the framework of the original scheme and some extension concerning both the class of Conservative and Non-conservative systems.

3.1. The framework of the original scheme

Let us consider a homogeneous system of non-linear, hyperbolic Conservative PDEs written as reported in Table 1, where $\mathbf{F}$ is the flux vector written as a function of the conserved vector $\mathbf{U}$. The relevant first order, finite volumes discretisation can be written in the form of Eq. (2) where, since the intercell flux is univocal, we can pose:

$$\mathbf{F}^{\pm}_{i+1/2}=\mathbf{F}_{i+1/2} \tag{14}$$

The quasi-linear form of this type of PDEs system is:

$$\frac{\partial\mathbf{U}}{\partial t}+\mathbf{A}_U\frac{\partial\mathbf{U}}{\partial x}=0 \tag{15}$$

where the matrix $\mathbf{A}_U=\partial\mathbf{F}/\partial\mathbf{U}$ is the Jacobian matrix of the conservative fluxes. Since the system is hyperbolic, $\mathbf{A}_U$ has a complete set of real eigenvalues λ_i and associated eigenvectors. Therefore, it can be diagonalised as:

$$\mathbf{A}_U=\mathfrak{R}\mathbf{\Lambda}\mathfrak{R}^{-1} \tag{16}$$

in which $\mathfrak{R}$ is the matrix of right eigenvectors, $\mathfrak{R}^{-1}$ is its inverse, and $\mathbf{\Lambda}$ is the diagonal matrix of the eigenvalues:

$$\mathbf{\Lambda}=\mathrm{diag}\left(\lambda_k\right)\quad;\quad k=1,\dots,N \tag{17}$$

Following Steger and Warming [35], we define a splitting of the previous matrix in the following form:

$$\mathbf{\Lambda}^{\pm}=\mathrm{diag}\left(\frac{1}{2}\left(\lambda_k\pm\left|\lambda_k\right|\right)\right)\quad;\quad k=1,\dots,N \tag{18}$$

such that $\mathbf{\Lambda}=\mathbf{\Lambda}^{+}+\mathbf{\Lambda}^{-}$. By substituting it in Eq. (16), the splitting $\mathbf{A}_U=\mathbf{A}_U^{+}+\mathbf{A}_U^{-}$ follows, where:

$$\mathbf{A}_U^{\pm}=\mathfrak{R}\mathbf{\Lambda}^{\pm}\mathfrak{R}^{-1} \tag{19}$$

In analogy to the so-called flux vector splitting method [35], the numerical scheme of Osher assumes that the flux vector $\mathbf{F}$ can be split into the two components $\mathbf{F}_+$ and $\mathbf{F}_-$ such that:

$$\mathbf{F}=\mathbf{F}_{+}+\mathbf{F}_{-} \tag{20}$$

where

$$\frac{\partial\mathbf{F}_{\pm}}{\partial\mathbf{U}}=\mathbf{A}_U^{\pm} \tag{21}$$

Denoting by $\mathbf{U}_i$ and $\mathbf{U}_{i+1}$ the initial values of the Riemann problem relevant to side $i+1/2$, then the corresponding numerical flux to be used in (2) is defined as:

$$\mathbf{F}_{i+1/2}=\mathbf{F}_{+}\left(\mathbf{U}_i\right)+\mathbf{F}_{-}\left(\mathbf{U}_{i+1}\right) \tag{22}$$

The evaluation of the right-hand terms appearing in the previous expression can be obtained by exploiting the following integrals of the Eq. (21) along a path connecting $\mathbf{U}_i$ to $\mathbf{U}_{i+1}$, representative of the relevant RP, in the phase space:

$$\mathbf{F}_{\pm}\left(\mathbf{U}_{i+1}\right)-\mathbf{F}_{\pm}\left(\mathbf{U}_{i}\right)=\int_{\mathbf{U}_{i}}^{\mathbf{U}_{i+1}}\mathbf{A}_{U}^{\pm}\,\mathrm{d}\mathbf{U} \tag{23}$$

Three different forms of $\mathbf{F}_{i+1/2}$ can be obtained in the following way:

- express $\mathbf{F}_{+}\left(\mathbf{U}_{i}\right)$ by using Eq. (23), substitute in Eq. (22) and then exploit the fact that $\mathbf{F}_{+}(\mathbf{U}_{i+1})+\mathbf{F}_{-}(\mathbf{U}_{i+1})=\mathbf{F}(\mathbf{U}_{i+1})$;
- express $\mathbf{F}_{-}\left(\mathbf{U}_{i+1}\right)$ by using Eq. (23), substitute in Eq. (22) and then exploit the fact that $\mathbf{F}_{+}(\mathbf{U}_{i})+\mathbf{F}_{-}(\mathbf{U}_{i})=\mathbf{F}(\mathbf{U}_{i})$;
- sum the results of the previous two forms.

For brevity, here we report only the last form, namely:

$$\mathbf{F}_{i+1/2}=\frac{1}{2}\left(\mathbf{F}_{i}+\mathbf{F}_{i+1}\right)-\frac{1}{2}\int_{\mathbf{U}_{i}}^{\mathbf{U}_{i+1}}\left|\mathbf{A}_{U}\right|\,\mathrm{d}\mathbf{U} \tag{24}$$

where

$$\left|\mathbf{A}_{U}\right|=\mathbf{A}_{U}^{+}-\mathbf{A}_{U}^{-} \tag{25}$$

The integral in equation (24) is usually called numerical viscosity, and to obtain a closed form, Osher and Solomon [27] proposed to build the phase path connecting the left and right RP states by using a specific set of integral curves and intermediate states. Since this procedure is not essential to understanding our work, we do not report it and address the reader to a suitable numerical manual (e.g., [28]) for details. What is important to note here is that the procedure is not readily applicable to any set of PDEs, and its success depends on the features of the system (e.g., the 2D shallow water case over horizontal bed by Zhao et al. [36] and the 1D shallow water equations over flat-bed with a passive tracer by Toro [37]).

3.2. The Dumbser-Toro scheme for Conservative systems

To overcome the difficulties of the original Osher scheme, Dumbser and Toro [26] exploited some properties of the path integration in the phase space. Let us define a *path* in the phase space as a continuous Lipschitz function $\boldsymbol{\psi}\left(s,\mathbf{U}_{i},\mathbf{U}_{i+1}\right)$ with $s\in[0,1]$ connecting the states $\mathbf{U}_{i}$ and $\mathbf{U}_{i+1}$ such that:

$$\boldsymbol{\psi}\left(0,\mathbf{U}_{i},\mathbf{U}_{i+1}\right)=\mathbf{U}_{i}\quad;\quad\boldsymbol{\psi}\left(1,\mathbf{U}_{i},\mathbf{U}_{i+1}\right)=\mathbf{U}_{i+1} \tag{26}$$

To simplify the notation, from here on, we will not explicitly indicate state dependency in the path.
Then, the integral in Eq. (24) can be written as:

$$\int_{\mathbf{U}_{i}}^{\mathbf{U}_{i+1}}\left|\mathbf{A}_{U}\right|\,\mathrm{d}\mathbf{U}=\int_{0}^{1}\left|\mathbf{A}_{U}\left(\boldsymbol{\psi}\left(s\right)\right)\right|\frac{\partial\boldsymbol{\psi}}{\partial s}\,\mathrm{d}s \tag{27}$$

and the relevant flux becomes:

$$\mathbf{F}_{i+1/2}=\frac{1}{2}\left(\mathbf{F}_{i}+\mathbf{F}_{i+1}\right)-\frac{1}{2}\int_{0}^{1}\left|\mathbf{A}_{U}\left(\boldsymbol{\psi}\left(s\right)\right)\right|\frac{\partial\boldsymbol{\psi}}{\partial s}\,\mathrm{d}s \tag{28}$$

Since $\mathbf{A}_{U}$ is the Jacobian of a conservative flux, the result of the integral is path-independent. Therefore, the authors propose the use of a path consisting of a simple straight line connecting the extremes of the considered RP:

$$\boldsymbol{\psi}\left(s\right)=\mathbf{U}_{i}+s\left(\mathbf{U}_{i+1}-\mathbf{U}_{i}\right) \tag{29}$$

In such a manner, the path derivative is $\partial\boldsymbol{\psi}/\partial s=\left(\mathbf{U}_{i+1}-\mathbf{U}_{i}\right)$ and can be brought outside the integral. Thus, Eq. (24) becomes:

$$\mathbf{F}_{i+1/2}=\frac{1}{2}\left(\mathbf{F}_{i}+\mathbf{F}_{i+1}\right)-\frac{1}{2}\left(\mathbf{U}_{i+1}-\mathbf{U}_{i}\right)\int_{0}^{1}\left|\mathbf{A}_{U}\left(\boldsymbol{\psi}\left(s\right)\right)\right|\,\mathrm{d}s \tag{30}$$

Since the integral is not in closed form, the authors propose to solve it numerically using the Gauss-Legendre quadrature rule, resulting in:

$$\mathbf{F}_{i+1/2}=\frac{1}{2}\left(\mathbf{F}_{i}+\mathbf{F}_{i+1}\right)-\frac{1}{2}\left(\mathbf{U}_{i+1}-\mathbf{U}_{i}\right)\sum_{j=1}^{G}\omega_{j}\left|\mathbf{A}_{U}\left(\boldsymbol{\psi}\left(s_{j}\right)\right)\right| \tag{31}$$

where ω_j is the weight associated with the Gaussian point s_j, and G is the number of employed points. As suggested by the authors, a good choice is $G = 3$, which approximates the integral well at a not-high computational cost.

3.3. The DOT scheme for Non-conservative systems

Dumbser and Toro [1] extended the Dumbser-Toro scheme, developed for the Conservative hyperbolic system, to Non-conservative hyperbolic systems. The scheme is briefly described further and is called the Dumbser-Osher-Toro (DOT) scheme.

Let us consider a Non-conservative, hyperbolic, homogeneous system of the type:

$$\frac{\partial \mathbf{U}}{\partial t} + \mathbf{H}_U \frac{\partial \mathbf{U}}{\partial x} = 0 \tag{32}$$

Following Castro et al. [38] and Parés [39], a path-conservative numerical scheme for Eq. (32) reads as:

$$\mathbf{U}_i^{n+1} = \mathbf{U}_i^n - \frac{\Delta t}{\Delta x}\left(\boldsymbol{\mathcal{F}}^-_{i+1/2} + \boldsymbol{\mathcal{F}}^+_{i-1/2}\right) \tag{33}$$

where $\boldsymbol{\mathcal{F}}^{\pm}_{i\mp1/2}$ are the fluxes at the interface between two adjacent cells and are defined by a given splitting of the integral of $\mathbf{H}_U$ along a path relative to the same interface. This condition, called *compatibility condition*, can be written as:

$$\boldsymbol{\mathcal{F}}^+_{i+1/2} + \boldsymbol{\mathcal{F}}^-_{i+1/2} = \int_0^1 \mathbf{H}_U\left(\boldsymbol{\psi}(s)\right) \frac{\partial \boldsymbol{\psi}}{\partial s}\, \mathrm{d}s \tag{34}$$

where it is implied that the path is relative to the interface $i + 1/2$.

A particular choice of the splitting allowed Dumbser and Toro [1] to obtain an expression that, in case of a conservative system and a linear path, reduces to the Dumbser-Toro scheme expressed by Eq. (30). In other words, the proposed splitting can be considered a generalisation of the Conservative case. The splitting can be obtained in the following way: exploiting the fact that the system is hyperbolic and, therefore, the matrix $\mathbf{H}_U$ is diagonalisable, assign to each flux one-half of the integral of Eq. (34) and then add or subtract one-half of the integral of $|\mathbf{H}_U| = \mathbf{H}_U^+ - \mathbf{H}_U^-$ along the same path. The resulting expression is:

$$\boldsymbol{\mathcal{F}}^{\pm}_{i+1/2} = \frac{1}{2}\int_0^1 \left(\mathbf{H}_U\left(\boldsymbol{\psi}(s)\right) \pm \left|\mathbf{H}_U\left(\boldsymbol{\psi}(s)\right)\right|\right) \frac{\partial \boldsymbol{\psi}}{\partial s}\, \mathrm{d}s \tag{35}$$

It is easy to demonstrate that these fluxes satisfy Eq. (34). Additionally, in the case of Conservative systems, where $\mathbf{H}_U = \partial \mathbf{F}/\partial \mathbf{U}$, the use of these expressions in Eq. (33) produces the same update algorithm given by the use of Eqs. (14) and (24) in Eq. (2), where $|\mathbf{A}_U|$ plays the role of $|\mathbf{H}_U|$.

To evaluate the integral, the authors propose using the same linear path and numerical strategy as in the Conservative case. With these choices, the final expression for the DOT fluxes reduces to:

$$\boldsymbol{\mathcal{F}}^{\pm}_{i+1/2} = \frac{1}{2}\left(\mathbf{U}_{i+1} - \mathbf{U}_i\right) \sum_{j=1}^{G} \omega_j \left(\mathbf{H}_U\left(\boldsymbol{\psi}\left(s_j\right)\right) \pm \left|\mathbf{H}_U\left(\boldsymbol{\psi}\left(s_j\right)\right)\right|\right) \tag{36}$$

Again, Dumbser and Toro [1] suggest using $G = 3$ since it produces good numerical results.

To express these fluxes according to the general scheme used in Eq. (2), it is sufficient to introduce the subsequent notation:

$$\mathbf{F}^{\pm}_{i+1/2} = \mp \boldsymbol{\mathcal{F}}^{\pm}_{i+1/2} \tag{37}$$

with which Eq. (35) can be rewritten as:

$$\mathbf{F}^{\pm}_{i+1/2} = \frac{1}{2}\int_0^1 \left(\mp \mathbf{H}_U\left(\boldsymbol{\psi}(s)\right) - \left|\mathbf{H}_U\left(\boldsymbol{\psi}(s)\right)\right|\right) \frac{\partial \boldsymbol{\psi}}{\partial s}\, \mathrm{d}s \tag{38}$$

and the corresponding expression in the case of linear path follows straightforwardly.

3.4. The DOT scheme for Combined systems

We can write the quasi-linear form of a Combined system in the following way:

$$\frac{\partial \mathbf{U}}{\partial t} + \mathcal{A}_U \frac{\partial \mathbf{U}}{\partial x} = 0 \tag{39}$$

where $\mathcal{A}_U = \mathbf{A}_U + \mathbf{H}_U$. Then, in principle, we can obtain the corresponding DOT-type flux by replacing, in Eq. (38), $\mathbf{H}_U$ and $\left|\mathbf{H}_U\right|$ with $\mathcal{A}_U$ and $\left|\mathcal{A}_U\right|$, respectively. However, it is useless to perform the numerical integral of $\mathbf{A}_U$ on a path, since, due to the conservative character of this matrix, the result is nothing but the difference in the physical fluxes evaluated at the boundary of the path, and these

Table 2
Table of symbols used to express Jacobians.

Symbol	Meaning	Independent variable
$\mathbf{A}_U$	$\partial\mathbf{F}/\partial\mathbf{U}$	$\mathbf{U}$
$\mathbf{A}_W$	$\partial\mathbf{F}/\partial\mathbf{W}$	$\mathbf{W}$
$\mathbf{B}_W$	$\partial\mathbf{U}/\partial\mathbf{W}$	$\mathbf{W}$

quantities are known. Furthermore, following Leibinger et al. [2], it is more convenient to write the fluxes in a form that resembles the Dumbser-Toro scheme, that is:

$$\mathbf{F}^{\pm}_{i+1/2} = \frac{1}{2}\left(\mathbf{F}_i + \mathbf{F}_{i+1}\right) - \frac{1}{2}\int_0^1 \left(\left|\mathcal{A}_U\left(\boldsymbol{\psi}\left(s\right)\right)\right| \pm \mathbf{H}_U\left(\boldsymbol{\psi}\left(s\right)\right)\right)\frac{\partial\boldsymbol{\psi}}{\partial s}\,\mathrm{d}s \tag{40}$$

This expression can be seen as a sum of the conservative flux expressed by Eq. (28), and the non-conservative one defined by Eq. (38) and represents a straightforward generalization of the DOT fluxes.

Finally, by using a linear path and a numerical integration with the Gauss-Legendre quadrature rule, we get the operational expression:

$$\mathbf{F}^{\pm}_{i+1/2} = \frac{1}{2}\left(\mathbf{F}_i + \mathbf{F}_{i+1}\right) - \frac{1}{2}\left(\mathbf{U}_{i+1} - \mathbf{U}_i\right)\sum_{j=1}^{G}\omega_j\left(\left|\mathcal{A}_U\left(\boldsymbol{\psi}\left(s_j\right)\right)\right| \pm \mathbf{H}_U\left(\boldsymbol{\psi}\left(s_j\right)\right)\right) \tag{41}$$

3.5. Possible variants

In the literature, some authors propose some variants to the DOT schemes described above. These variants are based on different ways to evaluate certain elements of the schemes. In particular:

- Castro et al. [40] propose three different approximations of the absolute value of $\mathcal{A}_U$ employing the Chebyshev polynomials or the Newman and the Halley functions. The obtained expressions provide good results with a limited numerical effort when the eigenstructure of the problem is complex.
- Carraro et al. [41] suggest avoiding pure numerical calculation of the eigenstructure of the problem when its closed form exists. In this way, the evaluation of the absolute value of the matrix would be less expensive. This procedure provides an optimised approach, but it could requires a lot of mathematical effort to obtain the eigenstructure and can be used only with the specific set of PDEs.
- Valiani and Caleffi [42] propose to use a path written in terms of the Riemann invariants. This choice could produce more complex and time-consuming integration since some models, such as the debris flow model, do not have an explicit version of the Riemann invariants.

4. DOT-type schemes for Hybrid systems

Compared to Non-conservative and Combined systems, Hybrid systems have certain peculiarities that require special treatment to be numerically discretised within the DOT methodology. The following Sections present our strategies for dealing with these features.

4.1. Reduction of Hybrid systems to a pseudo-Combined form

A possibility of dealing with Hybrid systems is to reduce them to a *pseudo-Combined* form, where the spatial derivative of the conserved variables vector replaces the spatial derivative of the primitive variables vector, and the matrix of non-conservative terms is defined appropriately, as described in the following paragraphs.

For the problems considered, the systems of PDEs are derived from mass and momentum balances using the physical (or primitive) variables (Section 2), so $\mathbf{U}$ can be expressed with a nonlinear transformation, as a function of $\mathbf{W}$. In this way, we can evaluate the Jacobian of the conserved variable with respect to the primitive variables $\mathbf{B}_W = \partial\mathbf{U}/\partial\mathbf{W}$. Thanks to the chain rule, the original non-conservative flux appearing in the Hybrid system can be rewritten in the following way:

$$\mathbf{H}_W\frac{\partial\mathbf{W}}{\partial x} = \mathbf{H}_W\frac{\partial\mathbf{W}}{\partial\mathbf{U}}\frac{\partial\mathbf{U}}{\partial x} = \mathbf{H}_W\mathbf{B}_W^{-1}\frac{\partial\mathbf{U}}{\partial x} \tag{42}$$

where $\partial\mathbf{W}/\partial\mathbf{U} = \mathbf{B}_W^{-1}$ is the inverse of matrix $\mathbf{B}_W$. Therefore, we can define the new matrix for the non-conservative terms as:

$$\hat{\mathbf{H}}_W = \mathbf{H}_W\mathbf{B}_W^{-1} \tag{43}$$

and we can obtain the following pseudo-Combined form:

$$\frac{\partial\mathbf{U}}{\partial t} + \frac{\partial\mathbf{F}}{\partial x} + \hat{\mathbf{H}}_W\frac{\partial\mathbf{U}}{\partial x} = 0 \tag{44}$$

Table 3
Synoptic table of the symbols used to express the matrices appearing in all the schemes presented. For the definition of $[\cdot]^{\pm}$, see Eq. (19).

Symbol	Meaning	Independent variable	Class
$\lvert\mathbf{A}_U\rvert$	$\mathbf{A}_U^+ - \mathbf{A}_U^-$	$\mathbf{U}$	Conservative
$\lvert\mathbf{H}_U\rvert$	$\mathbf{H}_U^+ - \mathbf{H}_U^-$	$\mathbf{U}$	Non-conservative
$\mathcal{A}_U$	$\mathbf{A}_U + \mathbf{H}_U$	$\mathbf{U}$	Combined
$\lvert\mathcal{A}_U\rvert$	$\lvert\mathbf{A}_U\rvert + \lvert\mathbf{H}_U\rvert$	$\mathbf{U}$	Combined
$\hat{\mathbf{H}}_W$	$\mathbf{H}_W\mathbf{B}_W^{-1}$	$\mathbf{W}$	Hybrid
$\hat{\mathbf{A}}_W$	$\mathbf{A}_W\mathbf{B}_W^{-1}$	$\mathbf{W}$	Hybrid
$\hat{\mathcal{A}}_W$	$\hat{\mathbf{A}}_W + \hat{\mathbf{H}}_W$	$\mathbf{W}$	Hybrid
$\lvert\hat{\mathcal{A}}_W\rvert$	$\lvert\hat{\mathbf{A}}_W\rvert + \lvert\hat{\mathbf{H}}_W\rvert$	$\mathbf{W}$	Hybrid

Nevertheless, as stated in the Introduction, even the conservative fluxes cannot be expressed as a function of the conserved variables, and therefore, it is not straightforward to write the relative quasi-linear form. We can overcome this situation by defining the Jacobian of the fluxes in terms of primitive variable $\mathbf{A}_W = \partial\mathbf{F}/\partial\mathbf{W}$, and we can use again the chain rule in the evaluation of the Jacobian of the fluxes in terms of primitive variables obtaining:

$$\hat{\mathbf{A}}_W = \frac{\partial\mathbf{F}}{\partial\mathbf{U}} = \frac{\partial\mathbf{F}}{\partial\mathbf{W}}\frac{\partial\mathbf{W}}{\partial\mathbf{U}} = \mathbf{A}_W\mathbf{B}_W^{-1} \tag{45}$$

The final quasi-linear form of the Hybrid system can then be recast into pseudo-Combined, quasi-linear form, namely:

$$\frac{\partial\mathbf{U}}{\partial t} + \hat{\mathcal{A}}_W\frac{\partial\mathbf{U}}{\partial x} = 0 \tag{46}$$

in which $\hat{\mathcal{A}}_W = \hat{\mathbf{A}}_W + \hat{\mathbf{H}}_W$. The similitude between this equation and Eq. (39) is evident, but it must stressed that in this last case, the matrix is a function of $\mathbf{U}$. Moreover, it is worth noting that even though $\hat{\mathcal{A}}_W$ is a function of the primitive variable vector, Eq. (46) is still in conservative form. Last but not least, the quasi-linear form of a Combined system, where we have $\mathcal{A}_U$, can always be rewritten in the pseudo-Combined, quasi-linear form, i.e. in terms of $\hat{\mathcal{A}}_W$, since the relation between conserved and primitive variables is always known.

For clarity, Tables 2 and 3 report a synoptic overview of the symbols used to express the Jacobians and the matrices appearing in all the schemes presented so far and which will be used later.

4.2. The DOT_{HCP} flux for Hybrid systems with Conserved Path

A DOT-type flux for Eq. (46) and its numerical evaluation can be borrowed from Eqs. (40) and (41), where we must substitute $\left\lvert\hat{\mathcal{A}_W}\right\rvert$ and $\hat{\mathbf{H}}_W$ instead of $\lvert\mathcal{A}_U\rvert$ and $\mathbf{H}_U$, respectively. The explicit expression of the fluxes becomes:

$$\mathbf{F}_{i+1/2}^{\pm} = \frac{1}{2}\left(\mathbf{F}_i + \mathbf{F}_{i+1}\right) - \frac{1}{2}\int_0^1 \left(\left\lvert\hat{\mathcal{A}}_W\left(\boldsymbol{\psi}\left(s\right)\right)\right\rvert \pm \hat{\mathbf{H}}_W\left(\boldsymbol{\psi}\left(s\right)\right)\right)\frac{\partial\boldsymbol{\psi}}{\partial s}\,\mathrm{d}s \tag{47}$$

while their numerical discretization is:

$$\mathbf{F}_{i+1/2}^{\pm} = \frac{1}{2}\left(\mathbf{F}_i + \mathbf{F}_{i+1}\right) - \frac{1}{2}\left(\mathbf{U}_{i+1} - \mathbf{U}_i\right)\sum_{j=1}^{G}\omega_j\left(\left\lvert\hat{\mathcal{A}}_W\left(\mathbf{W}\left(\boldsymbol{\psi}\left(s_j\right)\right)\right)\right\rvert \pm \hat{\mathbf{H}}_W\left(\mathbf{W}\left(\boldsymbol{\psi}\left(s_j\right)\right)\right)\right) \tag{48}$$

where the indication of the dependence of the matrices from the vector of primitive variables, which in turn depends on the path written for the vector of conserved variables, is explicit. This form allows us to understand how the computations must be performed: given a value of s_j, we compute the relative conserved vector, namely $\boldsymbol{\psi}(s_j) = \mathbf{U}(s_j)$ and, at this point, we have to numerically solve a nonlinear system to obtain $\mathbf{W}\left(\boldsymbol{\psi}(s_j)\right)$. Then, we can evaluate $\left\lvert\hat{\mathcal{A}}_W\left(\mathbf{W}\left(\boldsymbol{\psi}\left(s_j\right)\right)\right)\right\rvert$ and $\hat{\mathbf{H}}_W\left(\mathbf{W}\left(\boldsymbol{\psi}\left(s_j\right)\right)\right)$ and proceed with the subsequent steps. We call this DOT approach for Hybrid systems where the Path is evaluated in the Conserved variable phase space as DOT_{HCP} flux.

The computational cost of this pseudo-Combined approach is conceptually higher than a Combined approach, since the required passage from conserved to primitive variables is performed G times per flux. A possible way to overcome this drawback is presented in the next Section.

4.3. The DOT_{HPP} flux for Hybrid systems with Primitive Path

Our idea to avoid the recurrent and possibly costly shift from conserved to primitive variables in evaluating the path integral in the conserved-variable phase space was to recast the path in the primitive variables phase space. The implementation of our idea follows the subsequent steps:

1. rewrite the path integral in Eq. (47) in terms of conserved variables following the reverse operation performed to obtain Eq. (27); we get an expression of type:
$$\int_{\mathbf{U}_i}^{\mathbf{U}_{i+1}} [\cdot](\mathbf{W}(\mathbf{U}))\ \mathrm{d}\mathbf{U} \tag{49}$$
where $[\cdot]$ is a function of $\mathbf{W}$ through $\mathbf{U}$;
2. make a change of variable in the previous integral by exploiting the relation $\mathrm{d}\mathbf{U} = \partial\mathbf{U}/\partial\mathbf{W}\,\mathrm{d}\mathbf{W} = \mathbf{B}_W\,\mathrm{d}\mathbf{W}$, obtaining:
$$\int_{\mathbf{U}_i}^{\mathbf{U}_{i+1}} [\cdot](\mathbf{W}(\mathbf{U}))\ \mathrm{d}\mathbf{U} = \int_{\mathbf{W}_i}^{\mathbf{W}_{i+1}} [\cdot](\mathbf{W})\ \mathbf{B}_W(\mathbf{W})\ \mathrm{d}\mathbf{W} \tag{50}$$
where we have explicitly highlighted the dependency of the functions on $\mathbf{W}$;
3. define a path in the primitive-variables phase space as a continuous Lipschitz function $\boldsymbol{\phi}(s, \mathbf{W}_i, \mathbf{W}_{i+1})$, with $s \in [0,1]$, connecting the states $\mathbf{W}_i$ and $\mathbf{W}_{i+1}$ in this way:
$$\boldsymbol{\phi}(0, \mathbf{W}_i, \mathbf{W}_{i+1}) = \mathbf{W}_i \quad ; \quad \boldsymbol{\phi}(1, \mathbf{W}_i, \mathbf{W}_{i+1}) = \mathbf{W}_{i+1} \tag{51}$$
and, as before, to simplify the expression notation, from here on, we will not explicitly indicate the state dependency in the primitive variable path. We highlight that, since it exist a nonlinear transformation between the vectors of primitive and conserved variables, the path $\boldsymbol{\phi}$ is related to the path $\boldsymbol{\psi}$ by a suitable nonlinear transformation;
4. introduce this path in the integral, obtaining:
$$\int_{\mathbf{W}_i}^{\mathbf{W}_{i+1}} [\cdot](\mathbf{W})\ \mathbf{B}_W(\mathbf{W})\ \mathrm{d}\mathbf{W} = \int_0^1 [\cdot](\boldsymbol{\phi}(s))\ \mathbf{B}_W(\boldsymbol{\phi}(s))\ \frac{\partial\boldsymbol{\phi}}{\partial s}\ \mathrm{d}s \tag{52}$$

Exploiting this last result and using Eq. (43), we get the final expressions for the fluxes:

$$\mathbf{F}^{\pm}_{i+1/2} = \frac{1}{2}\left(\mathbf{F}_i + \mathbf{F}_{i+1}\right) - \frac{1}{2}\int_0^1 \left(\left|\hat{\mathcal{A}}_W(\boldsymbol{\phi}(s))\right| \mathbf{B}_W(\boldsymbol{\phi}(s)) \pm \mathbf{H}_W(\boldsymbol{\phi}(s))\right)\frac{\partial\boldsymbol{\phi}}{\partial s}\ \mathrm{d}s \tag{53}$$

By using a linear path in the Primitive-variable phase space, their numerical discretization become:

$$\mathbf{F}^{\pm}_{i+1/2} = \frac{1}{2}\left(\mathbf{F}_i + \mathbf{F}_{i+1}\right) - \frac{1}{2}\left(\mathbf{W}_{i+1} - \mathbf{W}_i\right)\sum_{j=1}^{G}\omega_j\left(\left|\hat{\mathcal{A}}_W\left(\boldsymbol{\phi}\left(s_j\right)\right)\right| \mathbf{B}_W\left(\boldsymbol{\phi}\left(s_j\right)\right) \pm \mathbf{H}_W\left(\boldsymbol{\phi}\left(s_j\right)\right)\right) \tag{54}$$

It is worth noting that the choice of a linear path in the Primitive-variables phase space in the DOT schemes is due to its simplicity and the arbitrariness of the choice of the path if physical constraints are unavailable. Nevertheless, this introduces an inconsistency between the Primitive-variable and the Conserved-variable approaches because, as already highlighted, the link between the two kinds of variables is not linear. Therefore, we expect a difference between the results obtained with this approach and those obtained with the DOT_{HCP} flux. We will estimate this difference in Section 5.2.

We call the DOT approach expressed by (54) for Hybrid systems where the Path is evaluated in the Primitive variables phase space as DOT_{HPP} flux.

4.4. Physical constraints and the DOT_{HZR} flux

In this Section, we focus on the possibility of expressing one of the terms of Eq. (53) considering certain physical constraints. The term is the following:

$$\int_0^1 \mathbf{H}_W(\boldsymbol{\phi}(s))\frac{\partial\boldsymbol{\phi}}{\partial s}\ \mathrm{d}s \tag{55}$$

and we are interested in possible constraints that should be considered in choosing the path.

The following analysis derives from that developed by Rosatti et al. [43] in the context of generalised Roe schemes. Let us consider a weak, discontinuous solution [16] of the pseudo-Combined quasi-linear system (46). According to the notation used so far, it can be written as follows:

$$\int_0^1 \left(-S_S \mathbf{I} + \hat{\mathcal{A}}_W\left(\hat{\boldsymbol{\phi}}(s)\right)\right) \mathbf{B}_W\left(\hat{\boldsymbol{\phi}}(s)\right) \frac{\partial \hat{\boldsymbol{\phi}}}{\partial s}\, \mathrm{d}s = 0 \tag{56}$$

where $\hat{\boldsymbol{\phi}} = \hat{\boldsymbol{\phi}}(s, \mathbf{W}_L, \mathbf{W}_R)$ is the path connecting the left and the right state of the discontinuous solution, and S_S is the speed of the moving discontinuity. We can expand the integral in this way:

$$\mathbf{F}_R - \mathbf{F}_L + \int_0^1 \mathbf{H}_W\left(\hat{\boldsymbol{\phi}}(s)\right) \frac{\partial \hat{\boldsymbol{\phi}}}{\partial s}\, \mathrm{d}s = S_S\left(\mathbf{U}_R - \mathbf{U}_L\right) \tag{57}$$

Comparing this expression with the one relevant to the GRH, namely Eq. (7), we can conclude that, across a discontinuity, the following relation holds:

$$\int_0^1 \mathbf{H}_W\left(\hat{\boldsymbol{\phi}}(s)\right) \frac{\partial \hat{\boldsymbol{\phi}}}{\partial s}\, \mathrm{d}s = -\mathbf{D}(\mathbf{W}_L, \mathbf{W}_R) \tag{58}$$

As in the original approach [43], we assume the validity of this equivalence in the integration of the non-conservative term over *the whole RP*, and not only across a single shock. This hypothesis implies the following assumptions:

- even though $\mathbf{D}$ is not constant in time [see, e.g. 32], we assume it as a given value inside a timestep (time linearisation) and is consistent with the invariance of the integral term implicitly assumed in the non-conservative approaches;
- the given value is calculated from the initial condition of the RP relevant to the considered cell interfaces.

The resulting relation is then:

$$\int_0^1 \mathbf{H}_W\left(\boldsymbol{\phi}(s)\right) \frac{\partial \boldsymbol{\phi}}{\partial s}\, \mathrm{d}s = -\mathbf{D}(\mathbf{W}_i, \mathbf{W}_{i+1}). \tag{59}$$

It is worth noting that for the models considered in this work, the previous expression is exact for fluid at rest and in steady condition, ensuring the well-balancing of the scheme.

From relation (59), we can deduce:

1. the path choice is not arbitrary, since not all paths satisfy Eq. (59). For example, using a linear path to evaluate the fluxes relevant to the overland flow model, namely:

$$\boldsymbol{\phi}(s) = \begin{cases} \phi_h = h_i + s\left(h_{i+1} - h_i\right) \\ \phi_u = u_i + s\left(u_{i+1} - u_i\right) \\ \phi_{z_b} = z_{b,i} + s\left(z_{b,i+1} - z_{b,i}\right) \end{cases} \tag{60}$$

   and using it to solve the integral (55), we end up with:

$$\int_0^1 \mathbf{H}_U\left(\boldsymbol{\phi}(s)\right) \mathbf{B}_W\left(\boldsymbol{\phi}(s)\right) \frac{\partial \boldsymbol{\phi}}{\partial s}\, \mathrm{d}s = \begin{bmatrix} 0 \\ g \dfrac{h_i + h_{i+1}}{2}\left(z_{b,i+1} - z_{b,i}\right) \\ 0 \end{bmatrix} \tag{61}$$

   which is not equal to the expression of $\mathbf{D}$ defined in Section 2.1.
2. finding a path that satisfy the constraint (59) may not be easy, and in any case, the use of the path may pose problems in integration. For example, Cozzolino et al. [44] proposed the following specific path that correctly reproduce the $\mathbf{D}$ term for the 1D overland flow model:

$$\boldsymbol{\phi}(s) = \begin{cases} \phi_h = \begin{cases} h_i - s\left(z_{b,i+1} - z_{b,i}\right) & ; s \in [0,1) \cup z_{b,i} \le z_{b,i+1} \\ h_{i+1} & ; s = 1 \cup z_{b,i} \le z_{b,i+1} \\ h_i & ; s = 0 \cup z_{b,i} > z_{b,i+1} \\ h_{i+1} - (1-s)\left(z_{b,i+1} - z_{b,i}\right) & ; s \in (0,1] \cup z_{b,i} > z_{b,i+1} \end{cases} \\ \phi_u = \text{not defined} \\ \phi_{z_b} = z_{b,i} + s\left(z_{b,i+1} - z_{b,i}\right) \end{cases} \tag{62}$$

Table 4
Table of the DOT-type fluxes proposed in this work for Hybrid systems and their distinguishing features.

Flux type	Distinguishing features
DOT_{HCP}	Linear path in the conserved variable phase space
DOT_{HPP}	Linear path in the primitive variable phase space Greater speed than DOT_{HCP}
DOT_{HZR}	Linear path in the primitive variable phase space Physical constraint Greater speed than DOT_{HPP} Greater accuracy than DOT_{HPP}

where the authors do not specify the path for the velocity variable since it is not mandatory for this specific non-conservative term. As can be seen, this path presents a discontinuity that is difficult to deal with.

3. it is useless to evaluate the integral using a numerical strategy since the value of $\mathbf{D}$ can be computed explicitly.

The last observation suggests a straightforward improvement of the flux expression given by Eqs. (53) and (54), by substituting the integral of $\mathbf{H}_W$ with the equivalent term $-\mathbf{D}$. This step leads to the following fluxes formulation:

$$\mathbf{F}^{\pm}_{i+1/2} = \frac{1}{2}\left(\mathbf{F}_i + \mathbf{F}_{i+1}\right) - \frac{1}{2}\int_0^1 \left|\hat{\mathcal{A}}_W\left(\boldsymbol{\phi}(s)\right)\right| \mathbf{B}_W\left(\boldsymbol{\phi}(s)\right) \frac{\partial \boldsymbol{\phi}}{\partial s}\, \mathrm{d}s \pm \frac{1}{2}\mathbf{D}(\mathbf{W}_i, \mathbf{W}_{i+1}) \tag{63}$$

and their numerical discretization:

$$\mathbf{F}^{\pm}_{i+1/2} = \frac{1}{2}\left(\mathbf{F}_i + \mathbf{F}_{i+1}\right) - \frac{1}{2}\left(\mathbf{W}_i + \mathbf{W}_{i+1}\right)\left(\sum_{j=1}^{G} \omega_j \left|\hat{\mathcal{A}}_W\left(\boldsymbol{\phi}(s_j)\right)\right| \mathbf{B}_W\left(\boldsymbol{\phi}(s_j)\right)\right) \pm \frac{1}{2}\mathbf{D}(\mathbf{W}_i, \mathbf{W}_{i+1}) \tag{64}$$

We call this DOT approach for a Hybrid system where the Path is evaluated in the Primitive-variables phase space, and a physical constraint is considered for the non-conservative term as DOT_{HZR} flux. We expect that this approach is slightly faster than the DOT_{HPP} scheme since the evaluation of $\mathbf{D}(\mathbf{W}_i, \mathbf{W}_{i+1})$ require less operations than the corresponding integral along a path. Moreover, we expect a greater accuracy than the DOT_{HPP} since the path integral present in this last approach can be considered an approximation of the term $\mathbf{D}(\mathbf{W}_i, \mathbf{W}_{i+1})$.

4.5. Applicability of the new $\text{DOT}_{H^{**}}$ approaches to other classes of systems

In this Section, we have presented three different approaches for Hybrid hyperbolic systems, whose peculiarities are reported in Table 4. Nevertheless, they can be applied to other Classes listed in Table 1, as described briefly hereafter.

We have already highlight in Section 3.3 that the DOT approach for Non-conservative systems reduces to the Dumbser-Toro approach for Conservative systems (Section 3.2). Therefore, we can consider the DOT approach as a generalization of the Dumbser-Toro one. Analogously, we can consider the DOT expressions for Combined systems a generalization of the DOT approach for Non-conservative systems.

Regarding the DOT_{HCP} flux, the possibility to write a Combined system in a pseudo-Combined form (as highlighted at the end of Section 4.1) also allows the applicability of this approach to Combined systems (please note that it is not possible to write a Hybrid system in a Combined form). Finally, as the DOT scheme, the DOT_{HCP} flux may be applied to Non-conservative and Conservative systems.

We can apply similar reasoning to the DOT_{HPP} flux, which also can be used for the numerical integration of Combined, Non-conservative and Conservative systems. Finally, we can state that the DOT_{HZR} flux can be applied both to Hybrid and Combined systems when a physical constraint regarding the non-conservative term is known.

5. Test cases concerning the Hybrid system of the debris flow model

In this Section, we present four test cases concerning the Hybrid system of the debris flow model in which the source term is disregarded. All tests consist of RPs, whose quasi-exact solution can be obtained following the technique proposed in Rosatti and Fraccarollo [32]. The values of the model parameter β (see Eq. (10)), left and right initial values and wave sequence in each RP are reported in Table 5. The other model parameters were considered constant and equal to $c_b = 0.65$ and $\Delta = 1.65$. In all the tests, the initial discontinuity was placed at $x = 0\,\text{m}$, the domain was discretized into constant cells of width $dx = 0.01\,\text{m}$, the simulation time was 2 seconds, and we used $CFL = 0.9$ as the stability condition. Finally, for all the schemes, we use three Gauss-Legendre points whose positions and weights are:

$$s_{1,3} = \frac{1}{2} \pm \frac{\sqrt{15}}{10}\ ;\ s_2 = \frac{1}{2} \quad ; \quad \omega_{1,3} = \frac{5}{18}\ ;\ \omega_2 = \frac{8}{18} \tag{65}$$

Table 5
Values of β parameter, initial values and wave sequence of the RPs test concerning the debris flow model.

Test case	β (−)	h_L (m)	h_R (m)	u_L (m/s)	u_R (m/s)	$z_{b,L}$ (m)	$z_{b,R}$ (m)	Wave sequence*
#1	0.2	2.000	0.595	0.100	0.115	0.000	0.202	RRS^+
#2	0.2	2.000	1.027	0.100	3.441	0.500	0.373	RRR
#3	0.1	1.000	0.958	3.000	0.653	0.000	−0.285	RS^+S^+
#4	0.05	1.000	0.702	3.000	1.896	0.000	0.476	S^-RS^+

* From left to right; $S^\pm$ means a shock moving in the positive or negative direction respectively, and R a rarefaction.

The first objective of these tests was to verify the capability of the proposed $DOT_{H^{**}}$ schemes to deal with this kind of problem and, secondly, to verify and quantify the distinguishing features of the approaches summarised in Table 4. Therefore,

- to quantify the accuracy of the numerical solutions obtained with DOT_{HPP} and DOT_{HZR}, for each Test, we have drawn the plots of the quasi-exact solution in terms of free-surface elevation (i.e., the flow depth added to the bed elevation), bed elevation and velocity, and the relative numerical solution obtained with the two methods. We emphasise that, for graphic clarity, we plotted one cell value for every forty-five. Additionally, we have drawn a zoomed-in plot of the velocity around each shock, where all cells are graphed, to highlight the differences between the solutions.
- to estimate the impact on the numerical solution of the different path types employed in the DOT_{HCP} and DOT_{HPP}, we have drawn the plots of the relative percentage difference between the two solutions for each Test. The relative percentage differences were computed in the following way:

$$\Delta h = \frac{h_{\text{HPP}} - h_{\text{HCP}}}{h_{\text{HPP}}} 100 \; ; \; \Delta u = \frac{u_{\text{HPP}} - u_{\text{HCP}}}{u_{\text{HPP}}} 100 \tag{66}$$

  where the subscripts refer to the relative flux type, while for the bed elevation:

$$\Delta z_b = \frac{z_{b\,\text{HPP}} - z_{b\,\text{HCP}}}{|\Delta z_b^0|} 100 \tag{67}$$

  where Δz_b^0 is the difference in bed height between the initial left and right values.
- to quantify the expected efficiency gain, we provide a table with the percentage speed gain of DOT_{HPP} over DOT_{HCP}, DOT_{HZR} over DOT_{HPP} and DOT_{HZR} over DOT_{HCP} obtained for each test. In particular, we indicate:

$$G_{\text{HCP-HPP}} = \frac{T_{\text{HCP}} - T_{\text{HPP}}}{T_{\text{HCP}}} 100 \; ; \; G_{\text{HPP-HZR}} = \frac{T_{\text{HPP}} - T_{\text{HZR}}}{T_{\text{HPP}}} 100 \; ; \; G_{\text{HCP-HZR}} = \frac{T_{\text{HCP}} - T_{\text{HZR}}}{T_{\text{HCP}}} 100 \tag{68}$$

  where $G_{x\text{-}y}$ is the percentage gain of method y over x and T_* is the averaged time employed to run the simulation with the $*$-flux.
- to quantify the influence of the grid resolution on numerical results obtained with DOT_{HZR}, for Test #1, we have drawn the plot of the quasi-exact solution in terms of velocity, and the relative numerical solutions obtained with a fine and coarse grid of respectively $dx = 0.01$ m and $dx = 0.1$ m resolution. We emphasise that, for graphic clarity, we plotted one cell value for every fifty cell for the fine grid, while for the coarse grid we plotted one cell every five. Additionally, we have drawn a zoomed-in plot of the velocity around the shock, where all cells are graphed, to highlight the differences between the solutions.
- to estimate the performance of the DOT_{HZR} flux in comparison with a non-DOT method already employed in the literature for the kind of problems faced in this paper, we considered the LHLL flux, an approximated and incomplete Riemann solver developed by Fraccarollo et al. [20]. We have drawn the plots of the relative percentage difference between the two numerical solutions for Test #1. The relative percentage differences were computed in the following way:

$$\Delta h = \frac{h_{\text{HZR}} - h_{\text{LHLL}}}{h_{\text{HZR}}} 100 \; ; \; \Delta u = \frac{u_{\text{HZR}} - u_{\text{LHLL}}}{u_{\text{HZR}}} 100 \; ; \; \Delta z_b = \frac{z_{b\,\text{HZR}} - z_{b\,\text{LHLL}}}{|\Delta z_b^0|} 100 \tag{69}$$

  where the subscripts refer to the relative flux type.

5.1. *Quasi-exact solutions vs DOT_{HPP} and DOT_{HZR} numerical solutions*

Figs. 2 and 3 show the comparison between the quasi-exact solution and the numerical results for Tests #1 and #2 and Tests #3 and #4, respectively. The proposed schemes approximate the quasi-exact solution rather well in all the cases and for all the variables, showing the accuracy and robustness of the approaches. Near the shocks are located the largest errors, where the two numerical solutions differ slightly. Fig. 4 allows a better analysis of the behaviour in these zones. In any case, the errors near the shocks are relatively small and are associated mainly with the shock speed. Additionally, the number of points necessary to approximate a shock is limited (generally less than ten). However, as expected, the DOT_{HRZ} scheme provides values that are, in any case, closer to the quasi-exact solution than the values of the DOT_{HPP} scheme. Along the rarefaction, the differences between the two schemes are negligible, as the contribution of the **D** term is marginal in these zones.

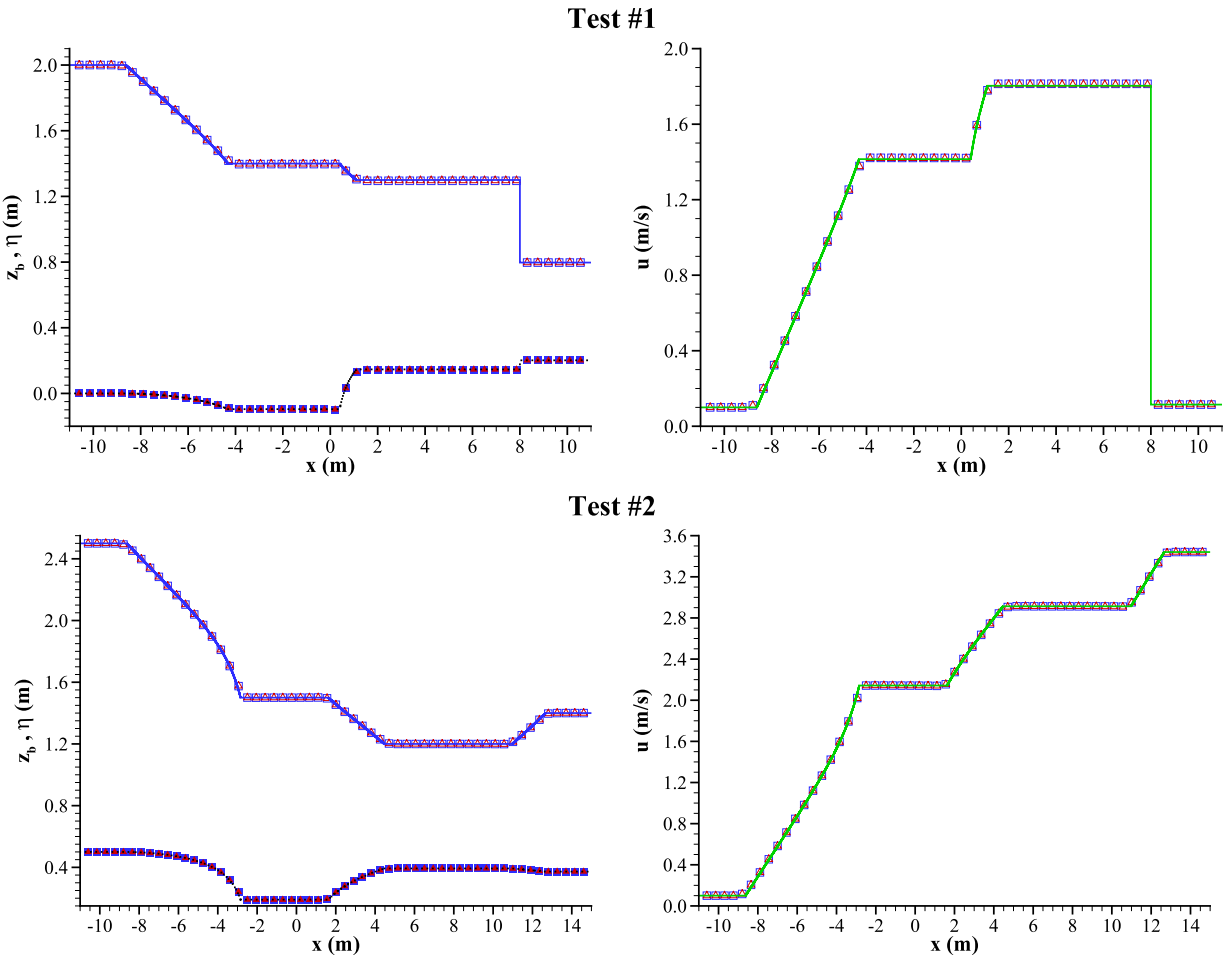

Fig. 2. Plots of the bottom elevation z_b and the free surface η (on the left) and of the velocity u (on the right) for Tests #1 and #2. Quasi-exact solutions for η and u in a continuous line, for z_b in a dotted line. Numerical solutions: □ DOT_{HPP} values; △ DOT_{HZR} values; filled symbols for z_b; empty symbols for η and u.

Table 6
Percentage efficiency gains, defined by Eq. (68), between the proposed DOT-type schemes, as a function of the Tests.

	Test #1	Test #2	Test #3	Test #4
$G_{HCP\text{-}HPP}$	3.63	3.85	3.77	3.67
$G_{HPP\text{-}HZR}$	0.42	0.56	0.44	0.37
$G_{HCP\text{-}HZR}$	4.03	4.39	4.20	4.03

5.2. *Differences between DOT_{HPP} and DOT_{HCP} numerical solutions*

Fig. 5 shows the relative percentage differences in the values of the numerical solutions obtained with the DOT_{HPP} and DOT_{HCP} schemes for each Test. The most significant errors are located around the shocks and are associated with the different positions of the wave rather than the different values before and after the shock. Elsewhere, the absolute value of the relative differences is less than 0.04%. This result suggests that the impact of the different path choices on the overall solution is nearly negligible. In other words, using the path in the primitive-variables phase space does not alter the overall accuracy of the DOT scheme employing the conserved-variables phase space.

5.3. *Efficiency gain analysis*

Table 6 reports the values of the percentage gains as defined by Eq. (68) and computed as the averaged value over ten runs. One can observe that the gains are almost independent of the type of test, and as expected, the DOT_{HPP} scheme is faster than DOT_{HCP}, while DOT_{HZR} is the fastest. Even if the gain values are not impressive (barely more than 4% with respect the DOT_{HCP}), using the DOT_{HZR} scheme allows us to reach simultaneously the maximum speed and accuracy without any particular effort.

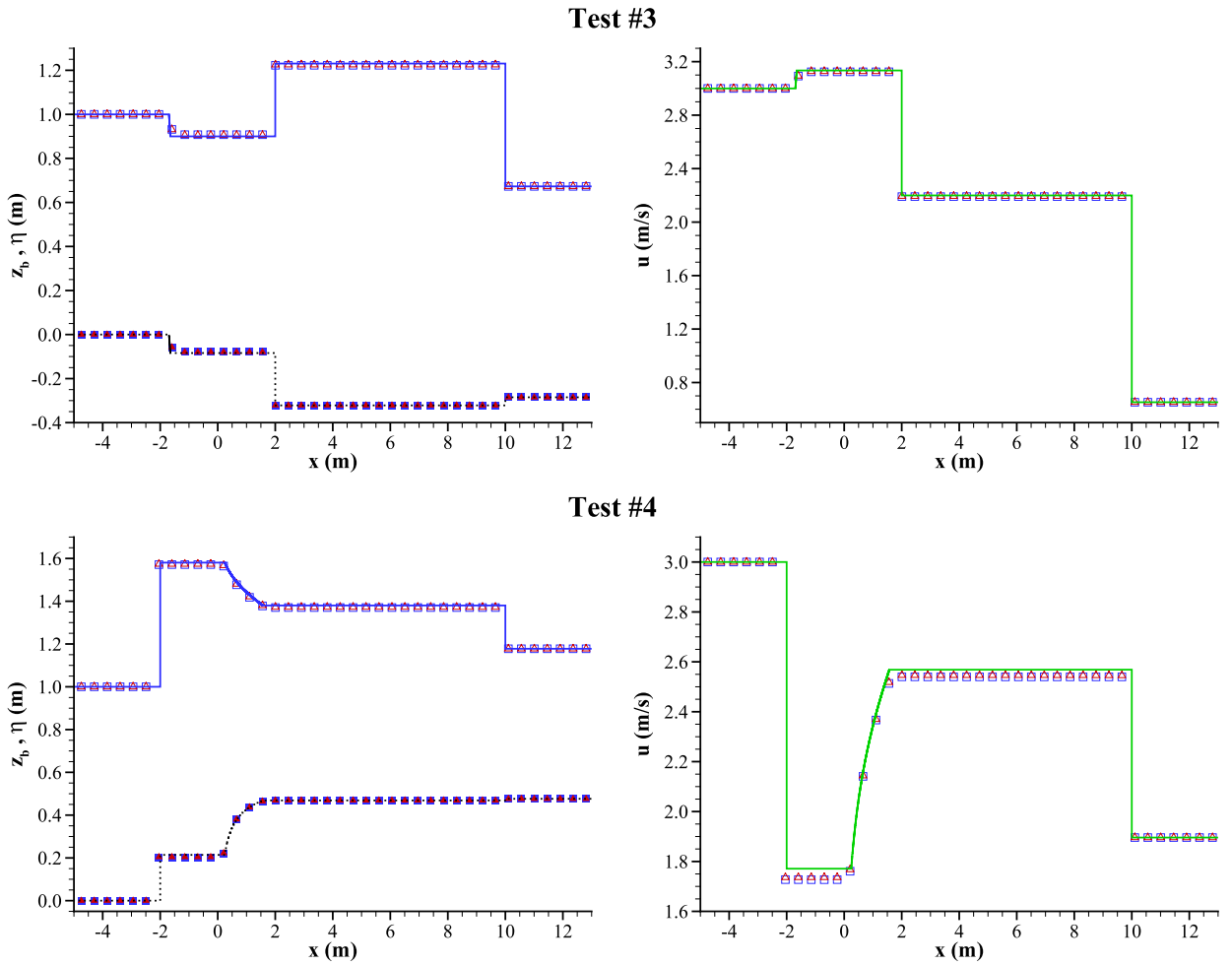

Fig. 3. Plots of the bottom elevation z_b and the free surface η (on the left) and of the velocity u (on the right) for Tests #3 and #4. Quasi-exact solutions for η and u in a continuous line, for z_b in a dotted line. Numerical solutions: □ DOT_{HPP} values; △ DOT_{HZR} values; filled symbols for z_b; empty symbols for η and u.

5.4. Coarse grid vs fine grid

Fig. 6 compares the quasi-exact solution and the numerical results for Test #1 obtained with the DOT_{HZR} scheme using a coarse and a fine grid. As expected, there is a lower definition of all the waves for the coarse grid results. The right panel of Fig. 6 allows a better analysis of the behaviour around the moving shock. The shock is essentially described by the same number of cells anyhow, using a coarse grid, the shock is spread over a larger space than with the fine grid. For the sake of brevity, we illustrated only Test #1, but the other Tests show similar behaviour.

5.5. Comparison between DOT_{HZR} and LHLL numerical solutions

Despite the speed of the LHLL flux being around 85% faster than the DOT_{HZR} one, the relative percentage differences in the values of the numerical solution are significant, and Fig. 7 shows this difference for Test #1. The main discrepancy is located around the shocks and is associated with the different positions of the wave rather than the dissimilar values before and after the shock (with the LHLL solution, the position of the shock is further away from the exact solution than the DOT_{HZR}). Also, a significant difference is present along the central rarefaction (for the bed elevation is more than 10%). Since the last wave is a discontinuity, it is not possible to define an order of convergence, and the assessment can only be qualitative. Again, for the sake of brevity, we illustrated only Test #1, but the other Tests show similar behaviour.

6. Test cases involving the Combined system of the overland flow model

In this Section, we present four test cases concerning the Combined system of the overland flow model in which the source term is disregarded. All tests consist of RPs whose quasi-exact solution can be obtained, again, following the technique proposed in Rosatti

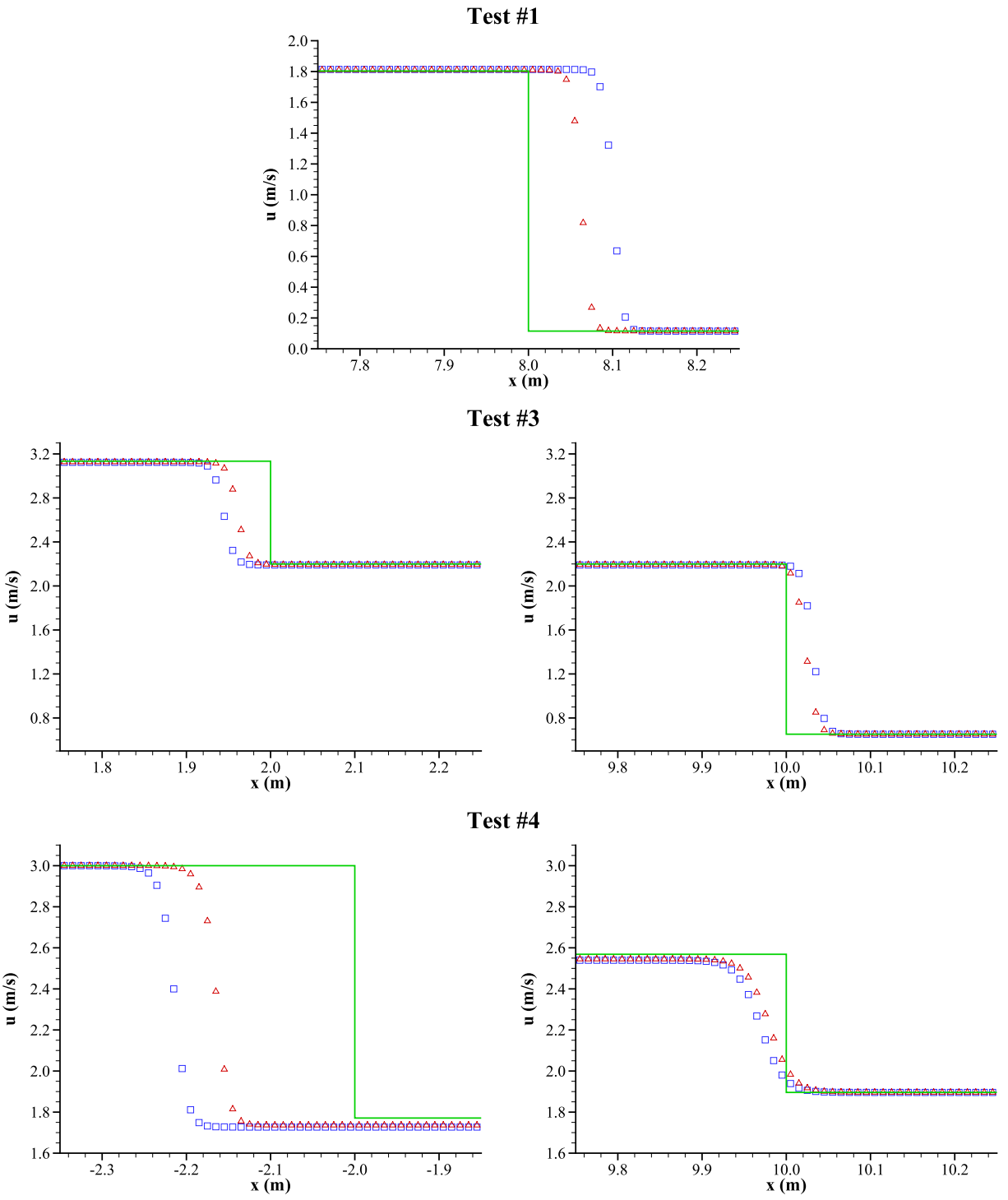

Fig. 4. Details of the velocity u near the moving shocks for all the Tests presenting this type of wave. Quasi-exact solutions in a continuous line; for the numerical solutions: □ DOT_{HPP} values; △ DOT_{HZR} values.

and Fraccarollo [32]. The values of the left and right initial values and wave sequence of each RP are reported in Table 7. As in the previous set of Tests, the initial discontinuity was placed at $x = 0\,\text{m}$, the domain was discretized into constant cells of width $dx = 0.01\,\text{m}$, the simulation time was 2 seconds, and we used $CFL = 0.9$ as the stability condition. For all the schemes, we use the same three Gauss-Legendre points used in the previous set of Tests.

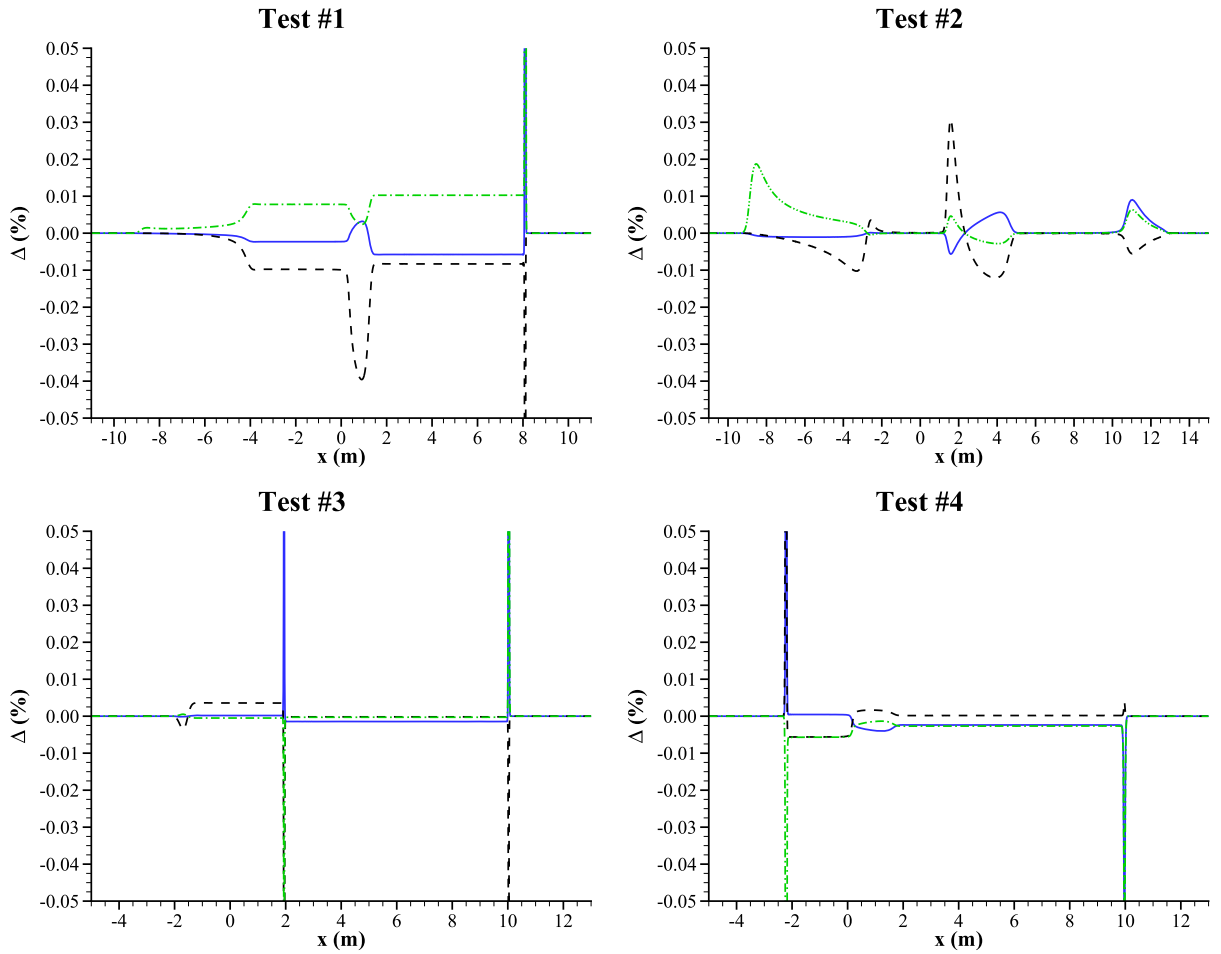

Fig. 5. Plots of the relative percentage differences $\Delta *$ between $\mathrm{DOT}_{\mathrm{HPP}}$ and $\mathrm{DOT}_{\mathrm{HCP}}$ for each Test. Δh in solid lines; Δz_b in dashed lines; Δu in dot-dashed lines. For definitions of the different $\Delta *$, see Eqs. (66) and (67).

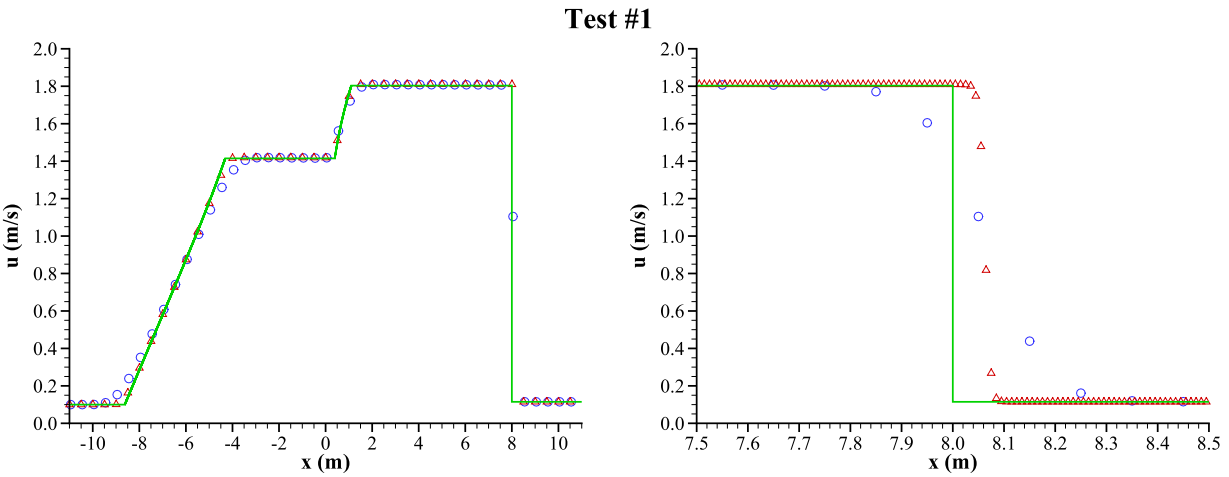

Fig. 6. Velocity u (left full plot, right details near the moving shock) for the Test #1. Quasi-exact solutions in a continuous line; for the numerical solutions: △ finer grid, ○ coarse grid.

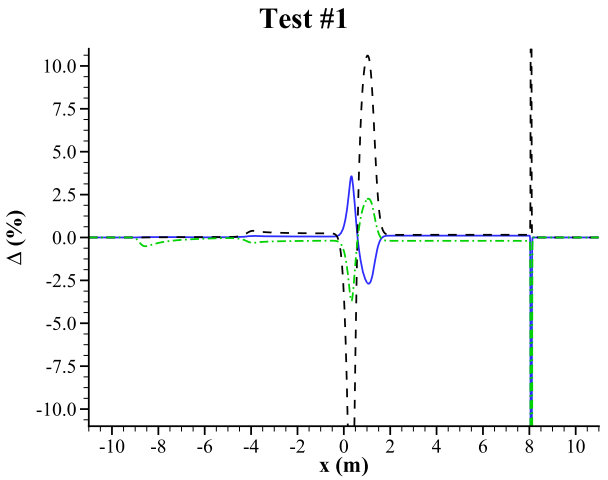

Fig. 7. Plots of the relative percentage differences $\Delta *$ between DOT_{HZR} and LHLL for Test #1. Δh in solid lines; Δz_b in dashed lines; Δu in dot-dashed lines. For definitions of the different $\Delta *$, see Eq. (69).

Table 7
Initial values and wave sequence of the RPs tests concerning the overland flow model.

Test case	h_L (m)	h_R (m)	u_L (m/s)	u_R (m/s)	$z_{b,L}$ (m)	$z_{b,R}$ (m)	Wave sequence*
#5	1.000	1.200	0.100	2.071	0.200	0.000	RCR
#6	1.000	0.731	0.000	0.251	0.300	0.000	RCS^+
#7	1.000	2.300	5.000	2.456	0.000	0.200	S^-CR
#8	1.000	1.436	5.000	0.863	0.200	0.300	S^-CS^+

* From left to right; $S^\pm$ means a shock moving in the positive or negative direction, respectively, R a rarefaction, and C a contact wave.

Since, as demonstrated in the previous Section, the difference between DOT_{HCP} and DOT_{HPP} is negligible, and we do not expect a significant difference in the computational speed, the goal of these tests is the comparison between the quasi-exact solution, the DOT_{HPP}, and the DOT_{HZR} schemes, to assess the possible effect of the analytical evaluation of the **D** term on the numerical solutions.

Figs. 8 and 9 show the comparison between the quasi-exact solution and the numerical results for Tests #5 and #6 and Tests #7 and #8, respectively, in term of free-surface elevation η and velocity u. The bed elevation z_b was plotted to comprehend the results better, even if it is only a dummy variable. For graphic clarity, we have drawn one cell value for every forty-five.

Analogously to the previous set of Tests, along the rarefaction waves, the numerical solutions deriving from both schemes are very similar and comparable to the quasi-exact solution. On the other hand, differently from the previous set of Tests, the differences between the numerical solutions around the contact waves are significant and can be appreciated without enlargements in Tests #5 and #6. Here, we notice that the DOT_{HZR} solution is far better than DOT_{HPP}. On the other hand, the differences between the two numerical solutions and the quasi-exact one are less evident in Tests #7 and #8. The reason for this dissimilar behaviour lies in the different importance of the term **D** in developing the RP since it acts only across the contact wave, as analyzed in various papers [e.g., 31,19]. Moreover, as the ratio of the bed step to the water depth at the lowest side of the step decreases, the importance of the term also decreases.

Comparing the results of this group of Tests with the ones of the previous set, we can notice that the DOT_{HZR} scheme performs better in the fixed-bed case than in the mobile-bed one. This performance is because in the overland flow, the wave across which the **D** is effective is a steady wave, and this condition matches with the assumption considered for the evaluation of the term. On the other hand, in the debris flow case, the wave across which **D** is effective is a mobile shock that is subjected to an unavoidable smoothing in the numerical solution, i.e. the shock is subdivided into a small number of moving jumps. Since the **D** term is not linear, this subdivision introduces an analytical error in the estimate of the overall term associated with the whole shock, and in turn, this generates a loss in the accuracy of the DOT_{HZR} scheme. Nevertheless, the DOT_{HZR} scheme reproduces the quasi-exact solution better than the DOT_{HPP} one.

7. Conclusions

In this paper, we have presented three different DOT-type approaches for the evaluation of the numerical fluxes in finite-volume schemes for Hybrid PDE systems arising from free-surface mobile-bed shallow-flow models. In addition, we also demonstrated their applicability to Combined systems associated, for example, with fixed-bed overland flows. The application of these approaches to different RPs, associated with a Hybrid problem and a Combined one, showed the accuracy and the efficiency of the developed schemes.

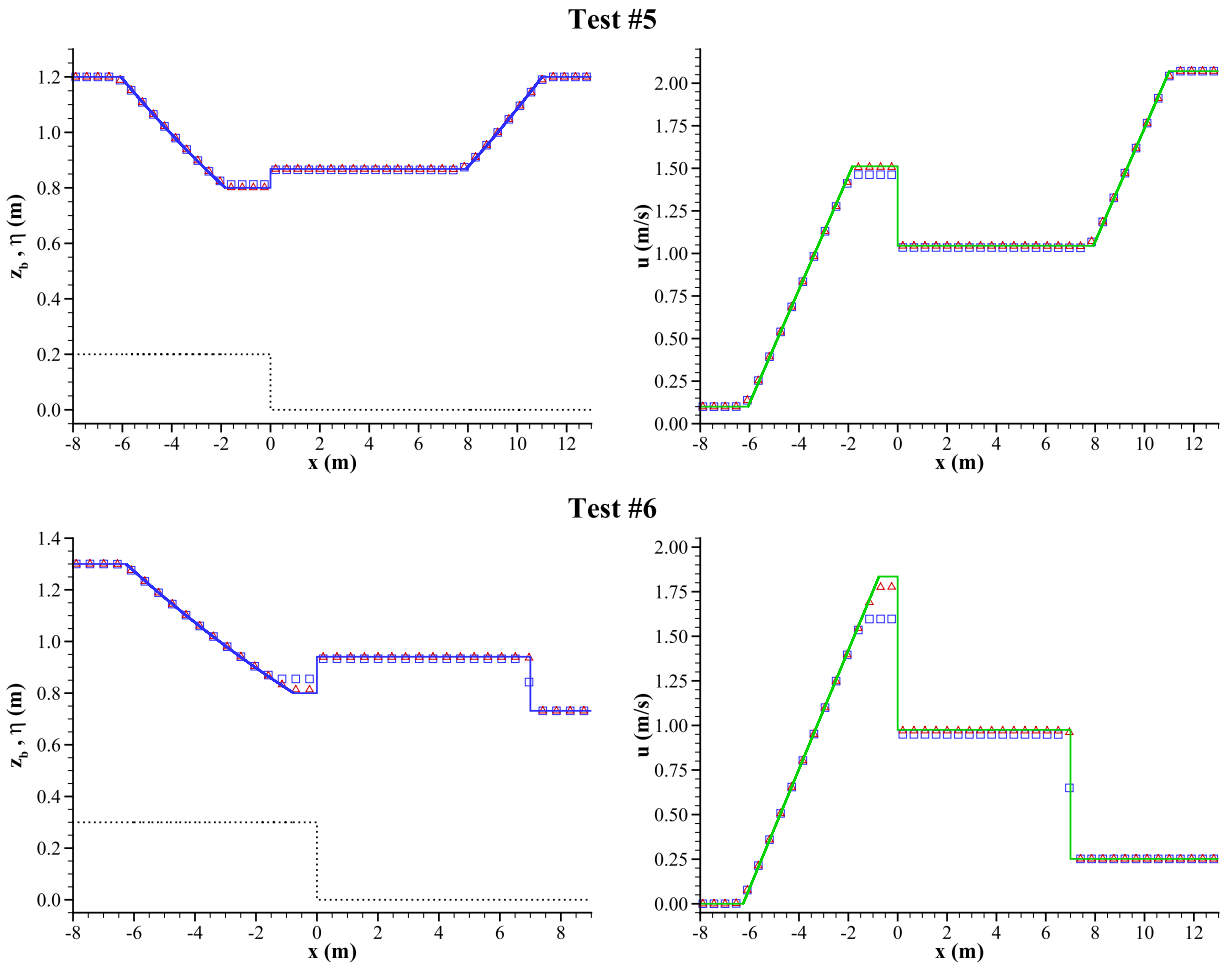

Fig. 8. Plots of the bottom elevation z_b and the free surface η (on the left) and of the velocity u (on the right) for Tests #5 and #6. Quasi-exact solutions for η and u in a continuous line, exact solution for z_b in a dotted line. Numerical solutions: □ DOT_{HPP} values; △ DOT_{HZR} values; z_b values not plotted, since they coincide with the exact solution.

What we can conclude from our work is:

- the DOT approach, initially developed for Non-conservative systems and later extended to Combined systems, can be further extended to Hybrid systems;
- our DOT-type fluxes share the same good features as the original DOT fluxes [1], namely:
  - they produce schemes that are accurate and robust despite their simplicity;
  - they use the eigenstructure of the PDEs system, which can be evaluated numerically if an explicit form is not available;
  - they are *complete* fluxes, as they exploit information from all the characteristic fields of the relevant RPs;
  - they do not need an entropy fix;
  - they are potentially well-suited for high-order implicit time-stepping schemes;
- in the case of explicit knowledge of the **D** term, the DOT_{HZR} scheme is the most accurate and efficient of the three schemes for both Hybrid and Combined systems. Furthermore, the test cases showed that the greater the bed discontinuity compared to the flow depth, the more accurate the DOT_{HZR} scheme is compared to the others;
- in the case where there is no explicit knowledge of the **D** term, the DOT_{HPP} scheme is more efficient than DOT_{HCP} because it avoids the passage from conserved to primitives in the evaluation of the integral along a path.

We want to highlight that the formulation of the DOT-type fluxes we have developed is quite general, and, therefore, can be applied not only to pure 1D problems (as in the present paper) but also to 2D cases without any change. Therefore, they can be used to produce robust and accurate numerical schemes for all the models described in the Introduction. In particular, we are interested in applying our new approach to operational tools for practitioners (like the WEEZARD system [45]) and for the analysis of complex free-surface flows such as the ones on which a culvert or bridge clogging occurs [46,47]. Additionally, if other more accurate physical descriptions of the **D** term are available in the future (e.g., in the case of free-surface vertical drops [48]), they

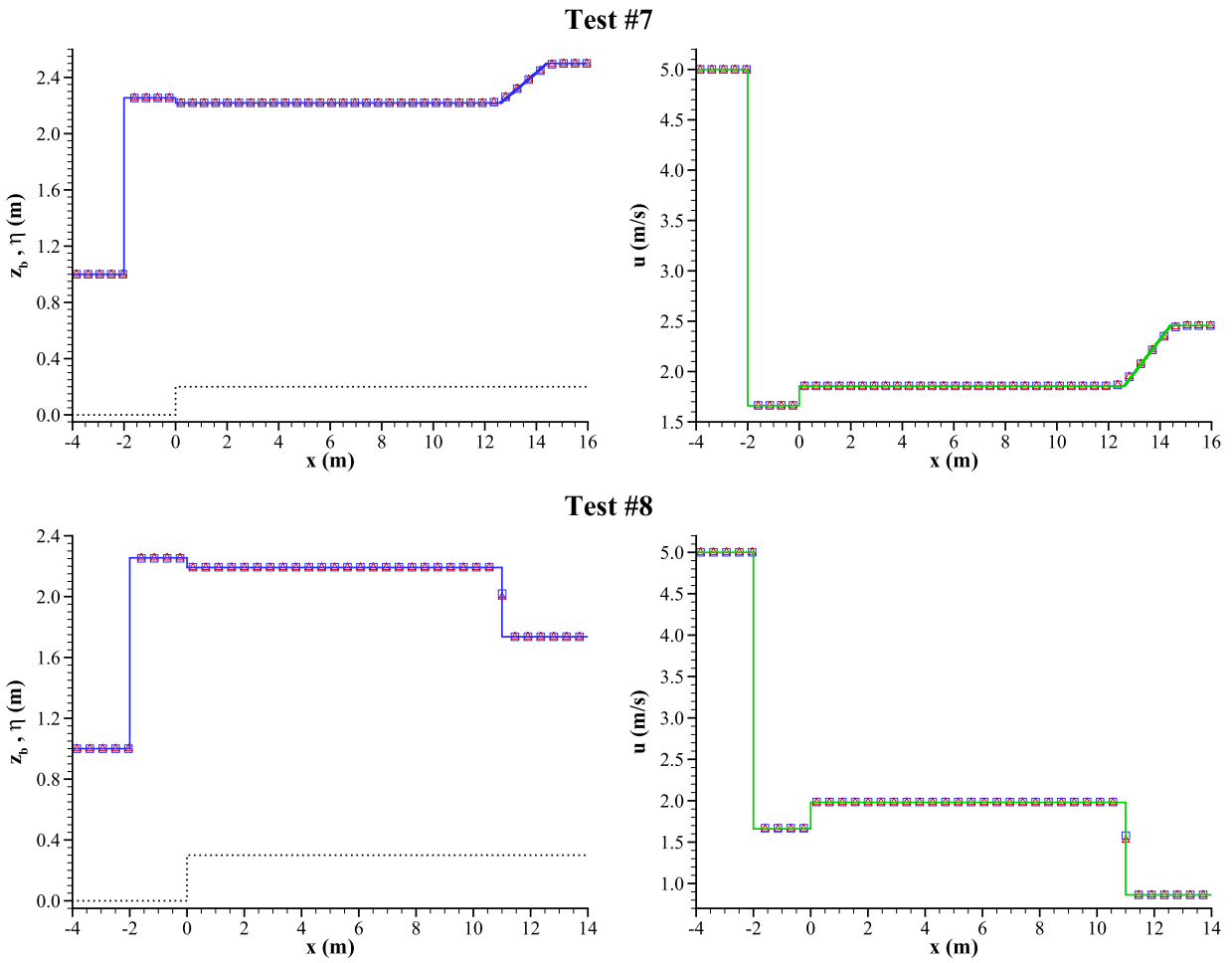

Fig. 9. Plots of the bottom elevation z_b and the free surface η (on the left) and of the velocity u (on the right) for Tests #7 and #8. Quasi-exact solutions for η and u in a continuous line, exact solution for z_b in a dotted line. Numerical solutions: □ DOT_{HPP} values; △ DOT_{HZR} values; z_b values not plotted, since they coincide with the exact solution.

may be used straightforwardly in the DOT_{HZR} scheme without any problem. Last but not least, again, due to its general formulation, the proposed schemes are ready to be applied to Hybrid and Combined problems with or without explicit formulation of the term **D** deriving from areas of physics other than the one used in this work, thus giving the novel approach a wide range of applicability.

CRediT authorship contribution statement

Daniel Zugliani: Conceptualization, Data curation, Formal analysis, Investigation, Methodology, Project administration, Software, Supervision, Validation, Visualization, Writing – original draft, Writing – review & editing. **Giorgio Rosatti:** Conceptualization, Data curation, Formal analysis, Funding acquisition, Methodology, Project administration, Resources, Software, Supervision, Validation, Writing – original draft, Writing – review & editing.

Declaration of competing interest

The authors declare that they have no known competing financial interests or personal relationships that could have appeared to influence the work reported in this paper.

Data availability

Data will be made available on request.

Acknowledgements

This research was partially funded by Caritro Foundation - Cassa di Risparmio di Trento e Rovereto within the project “Progetto WEEZARD: un sistema integrato di modellazione matematica a servizio della sicurezza nei confronti di pericoli idrogeologici in ambiente montano”. The authors would thank the anonymous revieweers for the comments and the helpful suggestions.

Appendix A. Eigenstructure of the overland flow model

The Jacobian of the conserved vector with respect to the primitive variables is:

$$\mathbf{B}_W = \frac{\partial \mathbf{U}}{\partial \mathbf{W}} = \begin{bmatrix} 1 & 0 & 1 \\ u & h & 0 \\ 0 & 0 & 1 \end{bmatrix} \tag{A.1}$$

while the Jacobian of the conserved fluxes with respect to the primitive variables is:

$$\mathbf{A}_W = \frac{\partial \mathbf{F}}{\partial \mathbf{W}} = \begin{bmatrix} u & h & 0 \\ u^2 + gh & 2gh & 0 \\ 0 & 0 & 0 \end{bmatrix} \tag{A.2}$$

From the previous two definitions, the matrix $\mathbf{A}_U$ is:

$$\mathbf{A}_U = \frac{\partial \mathbf{F}}{\partial \mathbf{U}} = \mathbf{A}_W \mathbf{B}_W^{-1} \begin{bmatrix} 0 & 1 & 0 \\ gh - u^2 & 2u & u^2 - gh \\ 0 & 0 & 0 \end{bmatrix} \tag{A.3}$$

and $\boldsymbol{\mathcal{A}}_U$ becomes:

$$\boldsymbol{\mathcal{A}}_U = \mathbf{A}_U + \mathbf{H}_U \begin{bmatrix} 0 & 1 & 0 \\ gh - u^2 & 2u & u^2 \\ 0 & 0 & 0 \end{bmatrix} \tag{A.4}$$

The eigenvalues and the associated eigenvectors for this model are the following:

$$\lambda_1 = u - \sqrt{gh} \Longleftrightarrow \begin{bmatrix} 1 \\ u - \sqrt{gh} \\ 0 \end{bmatrix} \tag{A.5}$$

$$\lambda_2 = 0 \Longleftrightarrow \begin{bmatrix} u^2 \\ 0 \\ u^2 - gh \end{bmatrix} \tag{A.6}$$

$$\lambda_3 = u + \sqrt{gh} \Longleftrightarrow \begin{bmatrix} 1 \\ u + \sqrt{gh} \\ 0 \end{bmatrix} \tag{A.7}$$

Appendix B. Eigenstructure of the debris flow model

A simple closed form of the three eigenvalues of the proposed debris flow model does not exist, so in the follow it is reported the characteristic polynomial of the homogeneous part of system (9) where the closure relation is expressed by equation (10):

$$2a_3\lambda^3 + 2ua_2\lambda^2 + a_1\lambda + 6u^3\beta a_0 = 0 \tag{B.1}$$

The coefficient a_i, for $i = 0, \dots, 3$, are the following:

$$a_3 = u^2\beta\left(2 + 3\Delta c_b\right) + ghc_b \tag{B.2}$$

$$a_2 = u^2\beta\left(\Delta\beta - 5 - 7\Delta c_b\right) - ghc_b\left(2 + \Delta\beta\right) \tag{B.3}$$

$$a_1 = u^4\beta\left(6 - 7\Delta\beta + 8\Delta c_b\right) + ghu^2\beta\left(\Delta c_b - 4\right) + 2ghc_b\left(u^2 - gh\right) \tag{B.4}$$

$$a_0 = \Delta u^2\beta + gh \tag{B.5}$$

Given a generic eigenvalue λ_i, solution of the characteristic polynomial, the associated eigenvector can be evaluated as follows:

$$\lambda_i \Longleftrightarrow \begin{bmatrix} \beta u^2\left(3u - 2\lambda_i\right) - gh\lambda_i c_b \\ \beta u^2\left(3u\lambda_i - 2\lambda_i^2 + 3\Delta\lambda_i c_b\left(u - \lambda_i\right)\right) - gh\lambda_i^2 c_b \\ 3u^2\beta c_b\left(u - \lambda_i\right) \end{bmatrix} \tag{B.6}$$

References

[1] M. Dumbser, E.F. Toro, A simple extension of the Osher Riemann solver to non-conservative hyperbolic systems, J. Sci. Comput. 48 (2011) 70–88, https://doi.org/10.1007/s10915-010-9400-3.

[2] J. Leibinger, M. Dumbser, U. Iben, I. Wayand, A path-conservative Osher-type scheme for axially symmetric compressible flows in flexible visco-elastic tubes, Appl. Numer. Math. 105 (2016) 47–63, https://doi.org/10.1016/j.apnum.2016.02.001.

[3] M. Christen, J. Kowalski, P. Bartelt, RAMMS: numerical simulation of dense snow avalanches in three-dimensional terrain, Cold Reg. Sci. Technol. 63 (2010) 1–14, https://doi.org/10.1016/j.coldregions.2010.04.005.

[4] D. Zugliani, G. Rosatti, TRENT2D®: an accurate numerical approach to the simulation of two-dimensional dense snow avalanches in global coordinate systems, Cold Reg. Sci. Technol. 190 (2021) 103343, https://doi.org/10.1016/j.coldregions.2021.103343.

[5] P. Costabile, C. Costanzo, F. Macchione, A storm event watershed model for surface runoff based on 2D fully dynamic wave equations, Hydrol. Process. 24 (2013) 554–569, https://doi.org/10.1002/hyp.9237.

[6] J. Singh, M.S. Altinakar, Y. Ding, Numerical modeling of rainfall-generated overland flow using nonlinear shallow-water equations, J. Hydrol. Eng. 20 (2015) 04014089, https://doi.org/10.1061/(asce)he.1943-5584.0001124.

[7] J. Fernández-Pato, D. Caviedes-Voullième, P. García-Navarro, Rainfall/runoff simulation with 2D full shallow water equations: sensitivity analysis and calibration of infiltration parameters, J. Hydrol. 536 (2016) 496–513, https://doi.org/10.1016/j.jhydrol.2016.03.021.

[8] J.S. O'Brien, P.Y. Julien, W.T. Fullerton, Two-dimensional water flood and mudflow simulation, J. Hydraul. Eng. 119 (1993) 244–261, https://doi.org/10.1061/(asce)0733-9429(1993)119:2(244).

[9] A. Armanini, L. Fraccarollo, G. Rosatti, Two-dimensional simulation of debris flows in erodible channels, Comput. Geosci. 35 (2009) 993–1006, https://doi.org/10.1016/j.cageo.2007.11.008.

[10] F. Bouchut, E.D. Fernández-Nieto, A. Mangeney, G. Narbona-Reina, A two-phase shallow debris flow model with energy balance, ESAIM: Math. Model. Numer. Anal. 49 (2015) 101–140, https://doi.org/10.1051/m2an/2014026.

[11] G. Rosatti, D. Zugliani, Modelling the transition between fixed and mobile bed conditions in two-phase free-surface flows: the composite Riemann problem and its numerical solution, J. Comput. Phys. 285 (2015) 226–250, https://doi.org/10.1016/j.jcp.2015.01.011.

[12] C. Di Cristo, M. Greco, M. Iervolino, A. Leopardi, A. Vacca, Two-dimensional two-phase depth-integrated model for transients over mobile bed, J. Hydraul. Eng. 142 (2016) 04015043, https://doi.org/10.1061/(ASCE)HY.1943-7900.0001024.

[13] S. Sansone, D. Zugliani, G. Rosatti, A mathematical framework for modelling rock-ice avalanches, J. Fluid Mech. 919 (2021) A8, https://doi.org/10.1017/jfm.2021.348.

[14] M. Ouda, E.A. Toorman, Development of a new multiphase sediment transport model for free surface flows, Int. J. Multiph. Flow 117 (2019) 81–102, https://doi.org/10.1016/j.ijmultiphaseflow.2019.04.023.

[15] S.P. Pudasaini, M. Mergili, A multi-phase mass flow model, J. Geophys. Res., Earth Surf. 124 (2019) 2920–2942, https://doi.org/10.1029/2019jf005204.

[16] G. Dal Maso, P.G. LeFloch, F. Murat, Definition and weak stability of nonconservative products, J. Math. Pures Appl. (9) 74 (1995) 483–548.

[17] I. Toumi, A weak formulation of Roe's approximate Riemann solver, J. Comput. Phys. 102 (1992) 360–373, https://doi.org/10.1016/0021-9991(92)90378-c.

[18] P.G. LeFloch, A.E. Tzavaras, Representation of weak limits and definition of nonconservative products, SIAM J. Math. Anal. 30 (1999) 1309–1342, https://doi.org/10.1137/s0036141098341794.

[19] C. Parés, E. Pimentel, The Riemann problem for the shallow water equations with discontinuous topography: the wet-dry case, J. Comput. Phys. 378 (2019) 344–365, https://doi.org/10.1016/j.jcp.2018.11.019.

[20] L. Fraccarollo, H. Capart, Y. Zech, A Godunov method for the computation of erosional shallow water transients, Int. J. Numer. Methods Fluids 41 (2003) 951–976, https://doi.org/10.1002/fld.475.

[21] J. Murillo, P. García-Navarro, Weak solutions for partial differential equations with source terms: application to the shallow water equations, J. Comput. Phys. 229 (2010) 4327–4368, https://doi.org/10.1016/j.jcp.2010.02.016.

[22] J. Murillo, P. García-Navarro, Augmented versions of the HLL and HLLC Riemann solvers including source terms in one and two dimensions for shallow flow applications, J. Comput. Phys. 231 (2012) 6861–6906, https://doi.org/10.1016/j.jcp.2012.06.031.

[23] M.J. Castro Díaz, J.A. López-García, C. Parés, High order exactly well-balanced numerical methods for shallow water systems, J. Comput. Phys. 246 (2013) 242–264, https://doi.org/10.1016/j.jcp.2013.03.033.

[24] G. Rosatti, L. Begnudelli, A closure-independent Generalized Roe solver for free-surface, two-phase flows over mobile bed, J. Comput. Phys. 255 (2013) 362–383, https://doi.org/10.1016/j.jcp.2013.08.020.

[25] M.J. Castro, J.M. Gallardo, A. Marquina, A class of incomplete Riemann solvers based on uniform rational approximations to the absolute value function, J. Sci. Comput. 60 (2014) 363–389, https://doi.org/10.1007/s10915-013-9800-2.

[26] M. Dumbser, E.F. Toro, On universal Osher-type schemes for general nonlinear hyperbolic conservation laws, Commun. Comput. Phys. 10 (2011) 635–671, https://doi.org/10.4208/cicp.170610.021210a.

[27] S. Osher, F. Solomon, Upwind difference schemes for hyperbolic systems of conservation laws, Math. Comput. 38 (1982) 339–374, https://doi.org/10.1090/s0025-5718-1982-0645656-0.

[28] E.F. Toro, Riemann Solvers and Numerical Methods for Fluid Dynamics: A Practical Introduction, third ed., Springer-Verlag, Berlin Heidelberg, 2009.

[29] M. Amaddii, G. Rosatti, D. Zugliani, L. Marzini, L. Disperati, Back-analysis of the Abbadia San Salvatore (Mt. Amiata, Italy) debris flow of 27-28 July 2019: an integrated multidisciplinary approach to a challenging case study, Geosciences 12 (2022) 385, https://doi.org/10.3390/geosciences12100385.

[30] P.G. LeFloch, M.D. Thanh, The Riemann problem for the shallow water equations with discontinuous topography, Commun. Math. Sci. 5 (2007) 865–885, https://doi.org/10.4310/cms.2007.v5.n4.a7.

[31] G. Rosatti, L. Begnudelli, The Riemann Problem for the one-dimensional, free-surface Shallow Water Equations with a bed step: theoretical analysis and numerical simulations, J. Comput. Phys. 229 (2010) 760–787, https://doi.org/10.1016/j.jcp.2009.10.010.

[32] G. Rosatti, L. Fraccarollo, A well-balanced approach for flows over mobile-bed with high sediment-transport, J. Comput. Phys. 220 (2006) 312–338, https://doi.org/10.1016/j.jcp.2006.05.012.

[33] A. Valiani, V. Caleffi, Momentum balance in the shallow water equations on bottom discontinuities, Adv. Water Resour. 100 (2017) 1–13, https://doi.org/10.1016/j.advwatres.2016.12.002.

[34] B. Engquist, S. Osher, One-sided difference approximations for nonlinear conservation laws, Math. Comput. 36 (1981) 321–351, https://doi.org/10.1090/s0025-5718-1981-0606500-x.

[35] J.L. Steger, R.F. Warming, Flux vector splitting of the inviscid gasdynamic equations with application to finite-difference methods, J. Comput. Phys. 40 (1981) 263–293, https://doi.org/10.1016/0021-9991(81)90210-2.

[36] D.H. Zhao, H.W. Shen, G.Q. Tabios, J.S. Lai, W.Y. Tan, Finite-volume two-dimensional unsteady-flow model for river basins, J. Hydraul. Eng. 120 (1994) 863–883, https://doi.org/10.1061/(asce)0733-9429(1994)120:7(863).

[37] E.F. Toro, Shock-Capturing Methods for Free-Surface, John Wiley & Sons, 2001.

[38] M. Castro, J.M. Gallardo, C. Parés, High order finite volume schemes based on reconstruction of states for solving hyperbolic systems with nonconservative products. Applications to shallow-water systems, Math. Comput. 75 (2006) 1103–1134, https://doi.org/10.1090/s0025-5718-06-01851-5.

[39] C. Parés, Numerical methods for nonconservative hyperbolic systems: a theoretical framework, SIAM J. Numer. Anal. 44 (2006) 300–321, https://doi.org/10.1137/050628052.

[40] M.J. Castro, J.M. Gallardo, A. Marquina, Approximate Osher-Solomon schemes for hyperbolic systems, Appl. Math. Comput. 272 (2016) 347–368, https://doi.org/10.1016/j.amc.2015.06.104.
[41] F. Carraro, A. Valiani, V. Caleffi, Efficient analytical implementation of the DOT Riemann solver for the de Saint Venant-Exner morphodynamic model, Adv. Water Resour. 113 (2018) 189–201, https://doi.org/10.1016/j.advwatres.2018.01.011.
[42] A. Valiani, V. Caleffi, Dam break in rectangular channels with different upstream-downstream widths, Adv. Water Resour. 132 (2019) 103389, https://doi.org/10.1016/j.advwatres.2019.103389.
[43] G. Rosatti, J. Murillo, L. Fraccarollo, Generalized Roe schemes for 1D two-phase, free-surface flows over a mobile bed, J. Comput. Phys. 227 (2008) 10058–10077, https://doi.org/10.1016/j.jcp.2008.08.007.
[44] L. Cozzolino, R. Della Morte, C. Covelli, G. Del Giudice, D. Pianese, Numerical solution of the discontinuous-bottom Shallow-water Equations with hydrostatic pressure distribution at the step, Adv. Water Resour. 34 (2011) 1413–1426, https://doi.org/10.1016/j.advwatres.2011.07.009.
[45] G. Rosatti, N. Zorzi, D. Zugliani, S. Piffer, A. Rizzi, A Web Service ecosystem for high-quality, cost-effective debris-flow hazard assessment, Environ. Model. Softw. 100 (2018) 33–47, https://doi.org/10.1016/j.envsoft.2017.11.017.
[46] M. Amaddii, G. Rosatti, D. Zugliani, L. Marzini, L. Disperati, Modelling stony debris flows involving culverted streams: the Abbadia San Salvatore case (Mt. Amiata, Italy), Rend. Online Soc. Geol. Ital. 61 (2023) 108–115, https://doi.org/10.3301/rol.2023.55.
[47] D. Zugliani, A. Ataieyan, R. Rocco, N. Betemps, P. Ropele, G. Rosatti, Bridge obstruction caused by debris flow: a practical procedure for its management in debris-flow simulations, E3S Web Conf. 415 (2023) 05031, https://doi.org/10.1051/e3sconf/202341505031.
[48] M.A. Gill, Hydraulics of rectangular vertical drop structures, J. Hydraul. Res. 17 (1979) 289–302, https://doi.org/10.1080/00221687909499573.